ORIGINAL ARTICLE

Oscillation Characteristics of Single Droplet Impacting Vertically on Smooth Surfaces Using Volume of Fluid Method

Zongjun Yin[1,2] · Rong Su[1] · Wenfeng Zhang[2] · Zhenglong Ding[1] · Futong Chai[1] · Qiannan Chen[1] · Qingqing Wang[1] · Fengguang Liu[3,4]

Abstract

The oscillation characteristics of a single droplet after normal collision with smooth surfaces are numerically investigated by using volume of fluid (VOF) method. An adaptive mesh refinement technique is used to guarantee the high computational accuracy of the interaction between the falling liquid droplet and the solid surface. The results of VOF simulations are consonant with the previously reported experiments. The effects of seven key issues on the oscillation characteristics of a liquid droplet advancing/recoiling onto both hydrophilic and hydrophobic surfaces are studied quantitatively with the help of dimensionless wetting length, average amplitude ratio and average oscillation period. These issues include impact velocity, contact angle, slip length, surface tension, droplet density, liquid viscosity and droplet diameter. Especially, surface and interface effects gradually become a primary factor that controls the droplet behavior as droplet size is reduced, and therefore the oscillation concerning micrometer-size droplet may be damped more rapidly. The presented study can contribute to provide more insight into the wetting kinetics of droplet collision, the interface interaction between the liquid droplet and the solid surface, and the oscillation features of the droplet spreading/receding after droplet impact.

Keywords Wetting kinetics · VOF approach · Droplet impact · Oscillation characteristics

Introduction

The fluid flow associated with a impinging droplet contains numerous interesting physical phenomena, and also arises abundant flow mechanism problems. Our work is primarily motivated by some practical applications and natural sciences, such as fuel injection, self-cleaning, pesticide spraying and raindrop splashing. Due to the pioneering work of Worthington (1876) and the developments of other previous researchers, a number of impact outcomes have been observed using experimental methods and numerical simulations. Rein (1993) described that the fluid dynamics of a liquid droplet impacting on a solid surface include bouncing, spreading and splashing. Rioboo et al. (2002) reported the first classification of the various outcomes of a droplet impact on different solid surfaces by experiments, and found that flow features primarily involve splashing, bouncing, partial rebound, deposition. The fluid mechanics of droplet impingement dynamics are quite complicated, despite its apparent simplicity. Here, several reviews demonstrated that these impact outcomes heavily rely on droplet properties (e.g. droplet density, surface tension, liquid viscosity), the types of target surface (e.g. solid surface, thin liquid film and deep liquid pool) and other impact conditions (e.g. impact velocity, droplet size, impact angle, surface roughness and wall temperature) (Mukherjee and Abraham 2007; Antonini et al. 2012; Gilet and Bush 2012; Sprittles and Shikhmurzaev 2012; Herbert et al. 2013; Liang and Mudawar 2016; Liang et al. 2019a, 2019b; Brandenbourger et al. 2017; Alabuzhev 2020). More

✉ Wenfeng Zhang
  wfzhang@mail.ustc.edu.cn

✉ Fengguang Liu
  liufg@buaa.edu.cn

1   School of Mechanical Engineering, Anhui Institute
    of Information Technology, Wuhu 241100, China

2   Institute of Photovoltaic, Southwest Petroleum University,
    Chengdu 610500, China

3   School of Integrated Circuit Science and Engineering,
    Hefei Innovation Research Institute, Beihang University,
    Hefei 230013, China

4   School of Integrated Circuit Science and Engineering,
    Beihang University, Beijing 100191, China

specifically, Yarin (2006) reviewed the splashing and the crown formation and propagation of a droplet impact on a thin liquid, and also reported spreading, fingering, splashing, receding, and rebounding when a droplet impacts on dry solid surfaces. Josserand and Thoroddsen (2016) studied the recent experimental and theoretical studies on a droplet hitting a solid surface, and indicated that surrounding gas is also one of the key interplays besides liquid density, surface tension and viscosity. Meanwhile, they also show that the lubrication pressure is an important contribution to the formation of entrapped bubble at droplet center. Liang and Mudawar (2017) reviewed the published literature addressing the fluid mechanics of a drop impacting onto a liquid film. His study mainly includes two aspects: the crown sheet, the ejecta sheet, and splashing for high-velocity impact; the phenomena of spreading, coalescence and rebound in low-velocity impact. On the other hand, experiments on a droplet impinging onto both curved surfaces and textured substrates have also been extensively investigated. Banitabaei and Amirfazli (2017) provided a comprehensive map of the droplet collision with extensive Weber number We (defined as $We = \rho_L D_0 V_0^2 / \gamma_{LV}$) on a spherical target. Here, ρ_L is the droplet density, D_0 is the droplet diameter, V_0 is the initial impact velocity and γ_{LV} is the surface tension coefficient. Liu et al. (2015) indicated that some surface profiles of asymmetric structure can promote the rapid bouncing of droplet. They found that the droplet striking on a cylindrical surface leads to about 40% contact time reduction. The droplet with shortened contact time is conducive to its practical applications, especially in anti-icing field. In addition, the surface designed to redistribute the droplet mass, momentum and energy has presented that the contact time can be further reduced by 50% (Bird et al. 2013; Gauthier et al. 2015; Song et al. 2017).

A small liquid droplet spreading on a horizontal solid surface will have a three-phase contact line at which a liquid/vapor interface meets the solid surface. Fluid mechanics argued that the stress and viscous dissipation near the contact line increase indefinitely because of the two-dimensional bi-harmonic equation coupled with no slip boundary condition. Huh and Scriven (1971) suggested that the influence of mathematical singularity in the vicinity of contact line can be eliminated by imposing slip boundary or adding long-range inter-molecular forces. Cox (1986) postulated that slip behavior can occur within the critical slip distance ε at the three-phase contact line, and then stress singularity is eliminated. However, pressure singularity remains in his theoretical research. Blake and De Coninck (2002) and Blake (2006) proposed that the molecules of gas phase are necessarily replaced by the liquid phase as a liquid advancing across rigid surfaces, which is called the molecule kinetic (MK) theory. This description indicates that both energy dissipation and

solid–liquid interaction force are finitely based on MK theory, respectively. Another important theory associated with respect to the moving contact line problem is diffuse-interface (DI) model. This model gets rid of a sharp, zero thickness fluid-gas interface with discontinuous quantities. Accordingly, this interface with non-zero, finite thickness is governed by the advective Cahn–Hilliard (CH) equation during the behavior evolution where quantities (e.g. density) vary smoothly but rapidly. Sibley et al. (2015) shown analytically that the stress components at the contact line vicinity are non-singular, and the pressure is finite in terms of DI model. Here, several papers (Pomeau 2002; Ren and Weinan 2007; Karimdoost-Yasuri and Passandideh-Fard 2013; Zhao 2014; Xie et al. 2016; Wang et al. 2020) are available, dealing with the advances of the contact line problem.

Numerical simulations of a droplet impacting onto solid surfaces have already obtained prodigious development during the last decade, which mainly includes interface tracking method and mesh-free method. The interface tracking method primarily contains volume of fluid approach (VOF), coupled level-set and VOF (CLSVOF), phase field dynamics (PFD) and Lattice-Boltzmann method (LBM). The mesh-free method basically involves smoothed particle hydrodynamics (SPH) and dissipative particle dynamics (DPD). More concretely, Malgarinos et al. (2014) performed VOF simulations and put forward a new adhesion force model of a droplet normally impacting on solid dry surfaces. They reported that this model dominated by capillary force provides a reasonable match with the experimental data during low We number (i.e., $We < 80$). Hasan et al. (2015) used a two-dimensional VOF simulations to investigate the deformation evolution of a droplet impacting on a solid surface for direct-print. Dupont and Legendre (2010) presented VOF simulations of the moving contact line for partially wetting liquids. Roisman et al. (2008) developed a new algorithm for modeling the dynamic contact angle in a VOF-based two-phase flow model. Šikalo et al. (2005) also made the similar investigation for the behaviour of the dynamic contact angle. Normally, the simulation result of CLSVOF method (coupled level-set function and VOF method) is more accurate than VOF method, because the LS function has a good advantage in calculating the curvature and the normal vector to the interface in terms of surface tension. For CLSVOF method, Zhu et al. (2018) investigated the impingement behaviors of three kinds of pesticide droplets spraying on the tea-surfaces. Guo et al. (2014) simulated a droplet impacting on a thin liquid film using CLSVOF, and captured bubble entrainment phenomenon. Li and Duan (2019) investigated the dynamics of a droplet impacting on an incline wetted surface, and also found the air entrapment, while Wang et al. (2018) studied a two dimensional

double droplet impacting on a moving liquid film. As to PFD method, this method applies chemical energy diffusion to overcome the moving contact line problem; that is, sharp interface limit and energy relaxation are used to demonstrate the fluid-wall interactions. Bai et al. (2008) performed three dimensional PFD simulations on droplet deformation in the micro-channel. They found that the mobility parameter has a major effect on the squeezing and breakup process of droplet motion with experimental validation. LBM method is a computational fluid dynamics method based on the Bolzmann equation, which is widely applied to simulate mesoscopic interactions, especially in the field of interface dynamics. Shen et al. (2012) mainly studied the influence of the impact velocity of a droplet advancing on curved surfaces with the LBM method, while Yin et al. (2018) performed the simulations of the oblique impingement of droplets on microstructured superhydrophobic surfaces. Gong and Cheng (2015) investigated the pool boiling heat transfer on smooth surfaces. Moreover, Yuan and Zhang (2016) investigated a droplet impacting on the randomly distributed rough surfaces. Finally, we pay special attention to the mesh-free method. Kordilla et al. (2013) employed multiphase SPH model to investigate the droplet flow on dry surfaces and surfaces prewetted with adsorbed films, and found that the trailing films of droplet flow may have a major influence on the average mass flux in the fracture. Meng et al. (2014) used SPH method to simulate the droplet spreading on porous substrates, where the advancing process was divided into two spreading stages: power-law inertial stage and viscous stage. Ma et al. (2017) simulated a single droplet impinging on different wall conditions using SPH method, and proposed a new splashing sub-model. For DPD approach, Chen et al. (2004) presented the shear flow evolution of polymer drops in a micro-channel. Li et al. (2013) studied the effect of the linear gradient of wettability in the droplet manipulation using DPD simulation. More recently, several studies also account for the mass and energy transfer mechanisms of the nano-sized droplet spreading on solid surfaces (Koplik and Zhang 2012; Li et al. 2015, 2017; Yin et al. 2019, 2020; Xu and Chen 2018, 2019), but these issues fall outside the scope of present discussion and will not be covered here.

Focusing on CFD simulations, most of the existing works study the ejecta formation and the crown radius evolution ratio for droplet impacting on liquid film, and the estimation of maximum spreading factor and the critical position of droplet breakup and splashing for droplet impacting on a solid surface. However, few works investigate the oscillation characteristics of a single droplet advancing/receding on both hydrophilic and hydrophobic surfaces, especially at the understanding and controlling oscillation of sub-millimeter sized droplet impact. Gunjal et al. (2005) studied the process of spreading/recoiling of a liquid drop after impact on a flat solid surface. Their result shown that the average contact angle reduces during the oscillations of a droplet. Deepu et al. (2014) investigated the oscillation mode and spectral response of sessile droplets on a vibrating substrate, and found the trend of the oscillation amplitude as a function of fluid viscosity and vibrational parameters. Zhou et al. (2018). focused on the oscillation characteristics after the head-on collision of two TiO_2-water nanofluid droplets, and considered the effects of impact velocity, drop size, and nanoparticle concentration. Inspired by these, efforts toward the effects of key parameters on the oscillation characteristics of droplet after normal collisions can improve some detailed explanations on mass and energy transfer mechanism problems. The main interest in the present study lies in the prediction and selection of the control strategies of droplet collision oscillation. Specifically, understanding of how the oscillation behavior of droplet impacting on a solid surface responds to the variations of control parameters can provides some feasible strategies to control its deposition and shape, and shorten the oscillation time for some potential applications. In this paper, we have carried out two-dimensional (2D) VOF simulations of a droplet impacting vertically on smooth surfaces. A dynamic adaptive mesh refinement technology is employed for capturing the small flow structures of droplet spreading. In addition, the generalized height-function (HF) curvature estimation is also used to accurately compute the interface curvature. It is worth mentioning that three-dimensional (3D) simulations modeling is superior to 2D modeling in visible analysis, but it also brings computational burden. According to the work of Hasan et al. (2015), Roisman et al. (2008) and Šikalo et al. (2005), a 2D modeling has been proved to be able to capture the basic physical features of a droplet impacting vertically on smooth surfaces, which is conducive to achieve a significant efficiency in computational cost. Our simulations are performed for the governing parameters of impact velocity, contact angle, slip length, surface tension, droplet density, liquid viscosity, and droplet diameter. More concretely, a single-variant analysis method is used to interpret the effect of these above-mentioned variables with the help of the dimensionless wetting length and the average oscillation period. In a word, the main objects of the present paper are to fully understand the effects of above-mentioned seven variables on the oscillation characteristics of a single droplet advancing/receding on both hydrophilic and hydrophobic surfaces. In addition, all VOF numerical simulations are performed with the Gerris program (a free software program for the solution of the partial differential equations describing fluid flow).

Method and Model

Computational Settings

The simulation system is a 2D simulation box with dimensions $L_x \times L_y = 2L \times L$, where the value of symbol L is equal to 8 mm, as shown in Fig. 1(a). The size of simulation domain is appropriate so that the droplet with diameter D_0 can spread freely. The initial distance h between the droplet and the solid surface is selected to be $h = D_0$. If the parameter value of h is too big, the impact velocity V_0 has low control accuracy and calculation consumption will increase. Conversely, the effect of gas-phase flow may be missed and the calculation error of solid-droplet interface is large, which means that the initial distance h should not be too small.

Governing Equation and Numerical Scheme

In the present study, the effect of the liquid compressible induced by droplet impacting on solid surfaces is neglected due to the fact that the timescale of the shock wave propagation across the droplet volume is very short (about $D_0/V_0 \times 10^{-4}$). Also, the compressible effect of gas is also ignored because the Mach number $Ma = V_0/c_0$ of gas-phase flow is $O(10^{-3})$ (c_0 denote the velocity of sound in the air).

Hence, the both fluids, a liquid and a gas, are assumed to be incompressible, Newtonian and to behave as laminar fluids. The surface tension γ_{LV} between these two fluids and the gravity are taken into account. In addition, we use ρ_V and μ_V to represent the density and viscosity of air, respectively. Accordingly, the characters ρ_L and μ_L are used to express droplet properties.

According to the VOF-based interface tracking approach, the immiscible liquid–gas two-phase flow spreading on the solid surface can be assumed to an effective fluid in the VOF calculation. Since the physical properties (e.g. density and viscosity) of each single phase flow are considered constant, the volume fraction variable c is used to track the phase fraction, density ρ and viscosity μ of this effective fluid. The phase fraction implies the gaseous phase when $c=0$, the liquid phase when $c=1$ and the interface region when c ranges between 0 and 1. More specifically, the density ρ can be expressed as $\rho = c\rho_L + (1-c)\rho_V$ using volume fraction variable c, and the viscosity μ can be defined as $= \mu c\mu_L + (1-c)\mu_V$. In this regard, the governing equations of this effective fluid flow involve the Navier–Stokes equation with surface tension term, the advection equation of phase fraction and the continuity equation, as follow:

$$\rho\left(\frac{\partial u}{\partial t} + u \cdot \nabla u\right) = -\nabla p + \nabla \cdot (2\mu D) + \rho g + \gamma_{LV}\kappa\delta n, \quad (1)$$
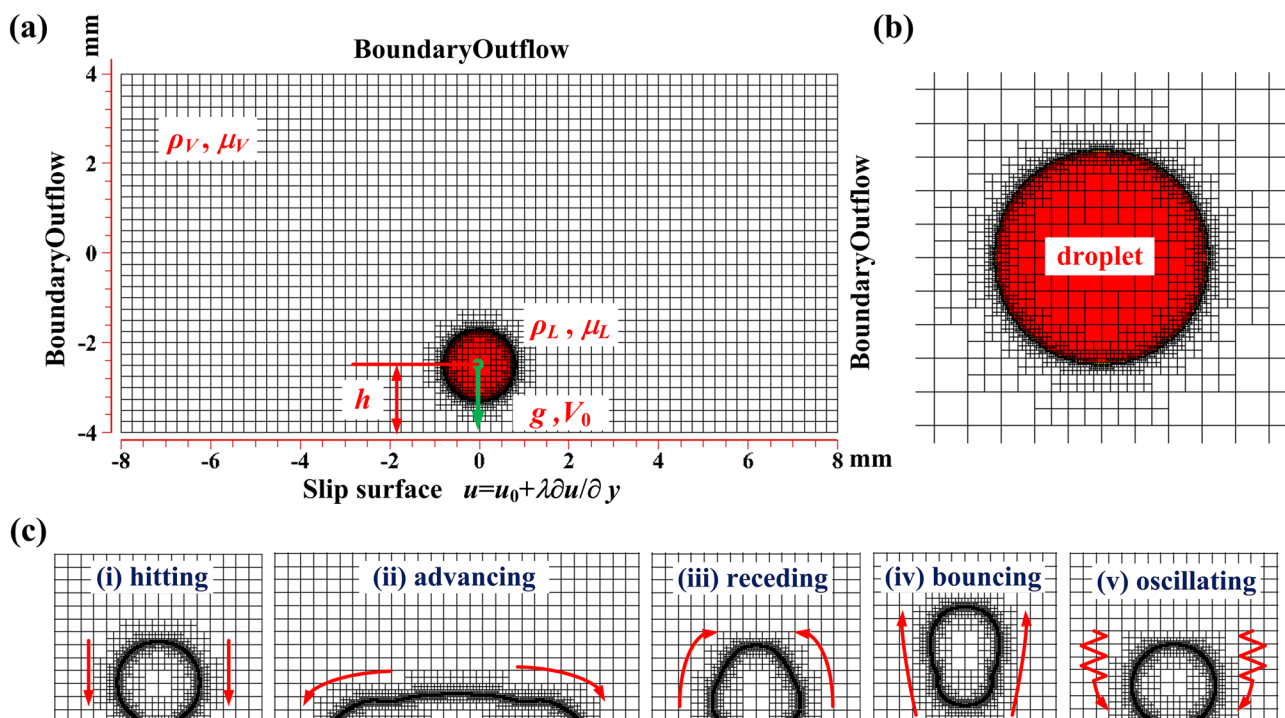

Fig. 1 (a) Schematic illustration of a single droplet impacting on smooth surfaces using Cartesian grid technique; (b) Depiction of a dynamic adaptive local Cartesian grid refinement for droplet; (c) Mesh pictures for the impingement dynamics behaviors of a droplet on smooth surfaces, including (i) hitting, (ii) advancing, (iii) receding, (iv) bouncing, and (v) oscillating

$$\frac{\partial c}{\partial t} + \nabla \cdot (cu) = 0, \tag{2}$$

$$\nabla \cdot u = 0, \tag{3}$$

where $\boldsymbol{u} \equiv (u, v)$ is the velocity vector, p is the pressure, and the second-order tensor $\boldsymbol{D}$ defines as $D_{ij} \equiv (\partial_i u_j + \partial_j u_i)/2$ and $\boldsymbol{g}$ is the gravity vector. The Dirac distribution function δ represents effect of the surface tension at the liquid–gas interface region; κ expresses the mean curvature of the interface, $\boldsymbol{n}$ denotes the unit normal of the interface going out from liquid phase.

The second-order accurate time discretisation of the volume-fraction/density and pressure can be found in the Popinet' work (Popinet 2003, 2009; Lagrée et al. 2011), as follow:

$$\rho_{n+\frac{1}{2}} \left[\frac{u_{n+1} - u_n}{\Delta t} + u_{n+\frac{1}{2}} \cdot \nabla u_{n+\frac{1}{2}} \right] = -\nabla p_{n+\frac{1}{2}} + \nabla \cdot \\ \left[\mu_{n+\frac{1}{2}} \left(D_n + D_{n+1} \right) \right] + \rho_{n+\frac{1}{2}} g + \left(\gamma_{LV} \kappa \delta n \right)_{n+\frac{1}{2}}, \tag{4}$$

$$\frac{c_{n+\frac{1}{2}} - c_{n-\frac{1}{2}}}{\Delta t} + \nabla \cdot (c_n u_n) = 0, \tag{5}$$

$$\nabla \cdot u_n = 0, \tag{6}$$

where subscripts n-1/2, n, n + 1/2 and n + 1 represent the corresponding time node, respectively. This governing system is further simplified using a classical time-splitting projection method (Popinet 2003), as follow:

$$\frac{\rho_{n+\frac{1}{2}}}{\Delta t} u_* - \nabla \cdot \left(\mu_{n+\frac{1}{2}} D_* \right) = \nabla \cdot \left[\mu_{n+\frac{1}{2}} D_n \right] \\ + \rho_{n+\frac{1}{2}} \left[\frac{u_n}{\Delta t} - u_{n+\frac{1}{2}} \cdot \nabla u_{n+\frac{1}{2}} \right] \\ + \rho_{n+\frac{1}{2}} g + \left(\gamma_{LV} \kappa \delta n \right)_{n+\frac{1}{2}}. \tag{7}$$

$$\frac{c_{n+\frac{1}{2}} - c_{n-\frac{1}{2}}}{\Delta t} + \nabla \cdot (c_n u_n) = 0, \tag{8}$$

$$u_{n+1} = u_* - \frac{\Delta t}{\rho_{n+\frac{1}{2}}} \nabla p_{n+\frac{1}{2}}, \tag{9}$$

$$\nabla \cdot u_{n+1} = 0, \tag{10}$$

where $\boldsymbol{u}_*$ is the auxiliary velocity field. According to Eqs. (9) and (10), we requires the solution of the following Poisson equation,

$$\nabla \cdot \left[\frac{\Delta t}{\rho_{n+\frac{1}{2}}} \nabla p_{n+\frac{1}{2}} \right] = \nabla \cdot u_*. \tag{11}$$

In order to achieve the decoupling of the pressure and the velocity field in the Eq. (11), an approximate projection approach is applied to obtain the velocity field $\boldsymbol{u}_{n+1}$ at time n + 1 using pressure correction (Popinet 2003). On the other hand, we would like to stress here that the expression of the surface tension term in Eq. (7) is composed of two terms representing, respectively the mean curvature κ and the phase interface location δn. According to Coutinuum-Surface-Force (CSF) approximation, these two term can be considered as $\delta n \approx \nabla c$ and $\kappa \approx \nabla \cdot \hat{n}$ ($\hat{n} = \nabla c / \|\nabla c\|$). Special attention should be paid to the accuracy of the curvature κ estimation. The generalized height-function (HF) curvature estimation technique on quad/octree discretisations is employed to handle the curvature κ calculation. This technique shows a hierarchy of consistent approximations, particularly when dealing with topology changes (Popinet 2003, 2009).

Combining Eq. (11), the momentum Eq. (7) can be reorganized as,

$$\frac{\rho_{n+\frac{1}{2}}}{\Delta t} u_* - \nabla \cdot \left(\mu_{n+\frac{1}{2}} D_* \right) = \nabla \cdot \left[\mu_{n+\frac{1}{2}} D_n \right] \\ + \rho_{n+\frac{1}{2}} \left[\frac{u_n}{\Delta t} - u_{n+\frac{1}{2}} \cdot \nabla u_{n+\frac{1}{2}} \right] \\ + \rho_{n+\frac{1}{2}} g + \left(\gamma_{LV} \kappa \delta n \right)_{n+\frac{1}{2}}. \tag{12}$$

This is an Helmholtz-type equation which can be solved using the multilevel Poisson solver described in Popinet (2009). The resulting Crank–Nicholson discretisation of the viscous terms is formally second-order accurate and unconditionally stable. The velocity advection term $\boldsymbol{u}_{n+1/2} \cdot \nabla \boldsymbol{u}_{n+1/2}$ is estimated using the Bell-Colella-Glaz second-order unsplit upwind scheme, which has been validated to be stable for CFL numbers smaller than one (Popinet 2009).

As to the droplet equilibrium, the discreted momentum equation can reduce to the following form:

$$\nabla p_{n+\frac{1}{2}} + \gamma_{LV} \kappa (\nabla c)_{n+\frac{1}{2}} = 0. \tag{13}$$

In order to solve the consistency problem of the discrete approximations of both gradient operators in Eq. (13), the surface-tension force is also used to correct the velocity field $\boldsymbol{u}_{n+1}$, which is identical to the implementation of the pressure field (see references Popinet 2003, 2009; Lagrée et al. 2011 for details).

Boundary Conditions and Dynamic Adaptive Grid Refinement

As shown in Fig. 1(a), BoundaryOutflow (a boundary condition used in Gerris program) boundary conditions are imposed on the left, right and top edges of simulation domain; that is, the values of p, u and v are equal to 0, respectively. Note that

the characters p, u and v denote the pressure, the velocity components in x and y directions, respectively. For bottom edge, the Navier slip boundary condition, defined as $u = u_0 + \lambda \partial u / \partial y$, is employed to describe the interaction between the solid surface and the droplet. Here λ is called the slip length, u_0 is the moving velocity of wall. Note that when zero normal derivative for the tangential component of vector fields and zero normal component of vector fields are imposed on the immobile wall, then it comes to the free-slip boundary condition. When a prescribed value of the contact angle θ_E at the wall is designated, the wall adhesion modifies the normal to the interface unit vector at the wall boundary cells $\hat{n}$ as

$$\hat{n} = \hat{n}_w \cos\theta_E + \hat{\tau}_w \sin\theta_E \qquad (14)$$

where $\hat{n}_w$ and $\hat{\tau}_w$ denote the unit vector normal and tangential to the wall, respectively.

In order to ensure the calculation accuracy of liquid–gas interface without increasing largely calculation burden, a dynamic adaptive local Cartesian grid refinement of the region around the moving droplet is employed. As observed in Fig. 1(b), a red area surrounded by the high resolution grid represents the droplet, where the value of VOF volume variable c is 1. The maximum and minimum levels of mesh refinement are specified to be 10 and 6, and the corresponding sizes of calculation cell are $L/2^{10}$ and $L/2^6$ (i.e., 7.8125×10^{-3} mm and 1.25×10^{-1} mm), respectively. According to droplet motion and shape deformation, the refinement level and cell position of the transitions are time-varying when an adaptive resolution varies along the droplet-gas interface. The interface criterion of adaptive refinement in a local cell can be expressed as follow:

$$\|c\| \Delta x / \max \|u\| > \delta , \qquad (15)$$

where $\|c\|$ is the value of VOF volume fraction variable c, Δx is the size of local cell, δ is a transition threshold and $\max\|u\|$ can be interpreted as the speed of a particle traveling cross the local cell. An important point is that cells will be coarsened only if $\|c\| \Delta x / \max\|u\|$ is smaller than $\delta/4$ at each time step. The threshold δ is designated to be 0.02 due to the fact that sharp variations of droplet-gas interface should correspond to high grid

(a)

0.0ms 1.6ms 4.0ms 6.8ms 8.8ms 10.8ms 11.2ms
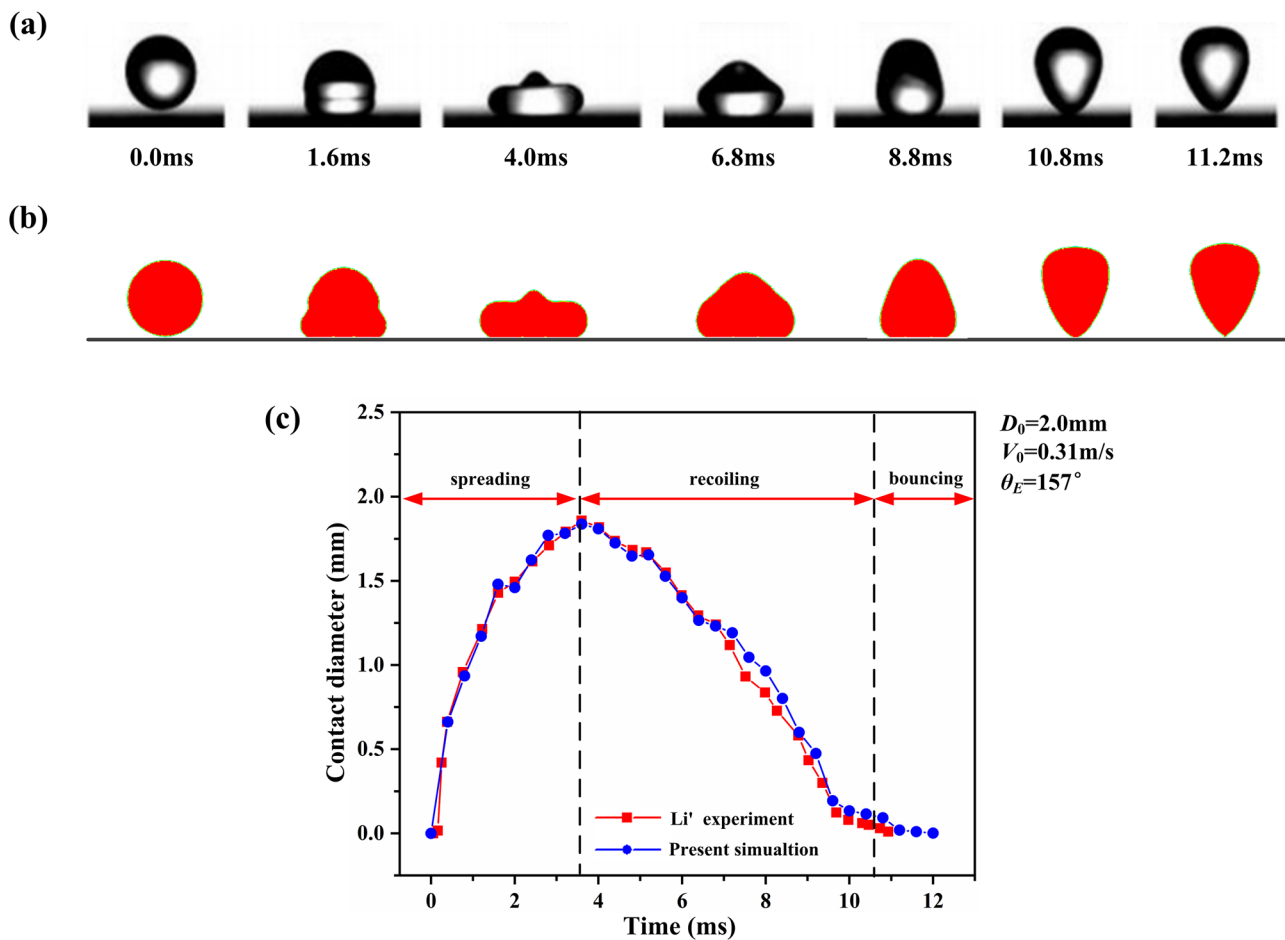
(b)

(c)

Fig. 2 (a) Experimental imaging of droplet bouncing-off. Adapted from the work of Li and Zhang (see Li and Zhang 2019); (b) Dynamic depiction of droplet rebounding using dynamic adaptive local grid refinement; (c) Time evolution of the droplet's wetting diameter

resolution. As shown in Fig. 1(c), the droplet dynamics, including hitting, advancing, receding, bouncing and droplet equilibrium after several oscillation periods, are presented. Meanwhile, the tracing technique of dynamic adaptive local Cartesian grid in the process of droplet deformation is also exhibited.

Validation

In order to further verify the dynamic performance of grid refinement, the temporal evolution of the normal collision of a water droplet (with $D_0 = 2.0$ mm and $V_0 = 0.31$ m/s) onto the solid super-hydrophobic surface (with static contact angle $\theta_E = 157°$ and free-slip boundary condition) is compared against experimental pictures from the work of Li and Zhang (2019). In the calculations, the density and viscosity of water and air are set as $\rho_L = 9.98 \times 10^2$ kg·m^{-3}/$\rho_V = 1.2$ kg·m^{-3}, $\mu_L = 1.003 \times 10^{-3}$ N·s·m^{-3}/$\mu_V = 1.8 \times 10^{-5}$ N·s·m^{-3}, respectively. The surface tension is set as $\gamma_{LV} = 7.5 \times 10^{-2}$ N·m^{-1}. As shown in Fig. 2(a), after the droplet experiences a spreading and receding process, it lifts off the solid surface completely at characteristic time t = 11.2 ms. Here, the maximum wetting diameter and its corresponding time are approximately 1.85 mm and 3.6 ms, respectively. The simulation results agree well with those obtained from experiments, and the only difference is a temporal advance of about 0.5 ms in Fig. 2(b). This difference is due to the fact that the effect of wall resistance (i.e., surface roughness) is neglected in the process of simulation. The numerical strategy can provide the accurate prediction of droplet deformation, and also makes a good solution to the problem of grid independence.

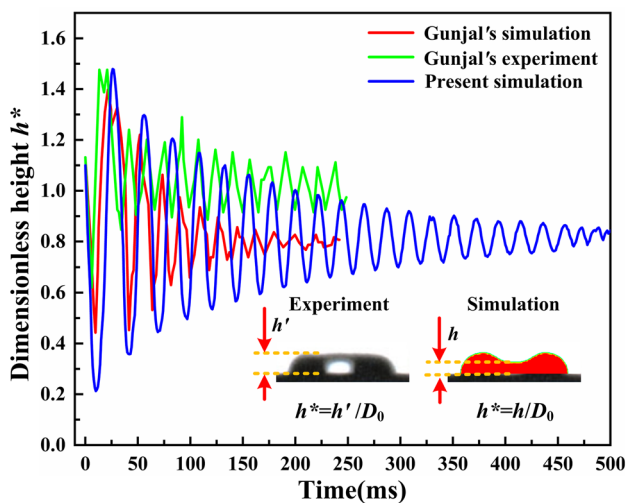As shown in Fig. 3, Gunjal et al. (2005) presented the temporal evolution of the droplet height with time for a water droplet (with diameter $D_0 = 2.5$ mm and impact velocity $V_0 = 0.3$ m/s) falling onto the Teflon surface (with static contact angle $\theta_E = 110°$), which is also used for the qualitative comparison with our simulations. It should be noted that the differences of dimensionless height between the experimental data (i.e., green line, $h^* = h'/D_0$, h' denote the maximum height of instantaneous shape of droplet) and simulated results (i.e., red line, $h^* = h/D_0$, h is the height of droplet center) in Gunjal' literature are likely due to the differences of measurement method, as presented in Fig. 3. Within time 100.0 ms of excluding the first oscillation cycle, the oscillations (beyond 465.0 ms) arising from droplet spreading and recoiling in their experiments imply that the average amplitude ratio χ as 1.032 and average oscillation period τ as 18.12 ms. The blue curve obtained from our calculations behaves as a damped oscillation, which is damped out until 500.0 ms. Our calculations indicate that the average amplitude ratio χ and the average oscillation period τ are 1.051 and 18.33 ms, respectively, which is consistent with the Gunjal' works. In addition, the maximum dimensionless height during the first oscillation cycle is found to be 1.48, which is also in agreement with the experimental values (i.e., 1.48).

Results and Discussion

Effects of Impact Velocity on the Droplet Oscillation

After impinging on a solid surface, the droplet leads to either bouncing-off, splashing or adhering, which largely depends on the impact velocity. In this regard, impact velocity V_0 should be treated as the first key parameter to study the oscillation features of a water droplet spreading/receding on a smooth surface with the free-slip boundary condition. The impact velocity can not be too large, otherwise the droplet may lift off the solid surface or splashing occurs. Therefore, five different impact velocities of $V_0 = 0.1$ m/s, 0.2 m/s, 0.3 m/s, 0.4 m/s and 0.5 m/s are considered here. In addition, the diameter of water droplet is designated as $D_0 = 1.6$ mm and the static contact angle is $\theta_E = 90°$.

Figure 4(a) presents the images at various times for droplets with five different impingement velocities (relatively small) impacting on an ideal smooth surface. Figure 4(b) presents the first oscillation cycle of the spreading factor β (defined as $\beta = L/D_0$, L is the current wetting length) with time, which is in favor of acquiring the maximum spreading factor β_{max}. The time node t = 0.0 ms is set as the droplet immediately touches the ideal surface for all test cases, and the spreading factor is zero at this moment. For a lower velocity of $V_0 = 0.1$ m/s (see Fig. 4(a)-i), we can see that the droplet experiences the spreading and retracting stages. At the beginning of droplet collision,
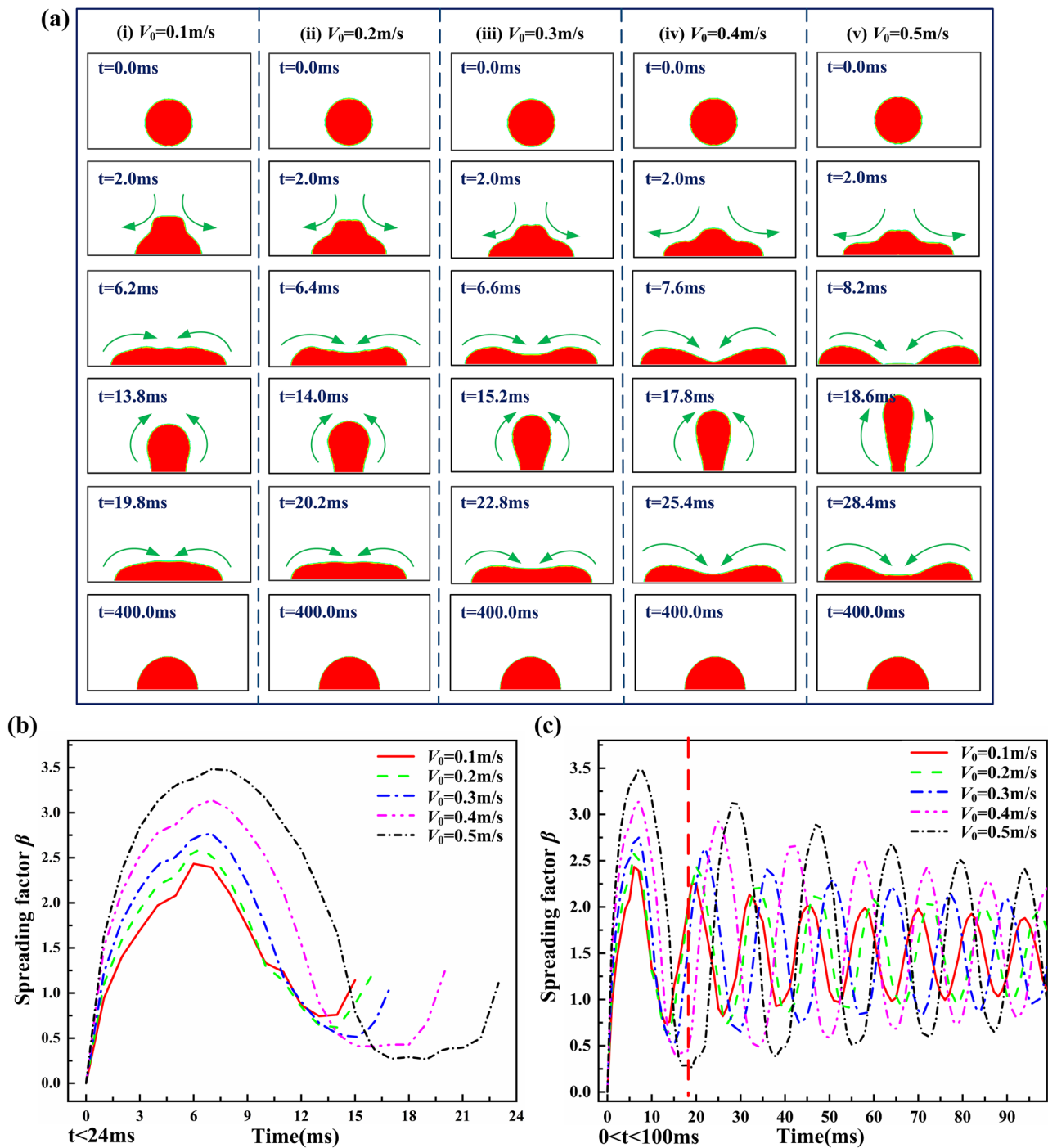

Fig. 3 Quantitative comparisons of the Gunjal' data (see Gunjal et al. 2005) of droplet height variations with the present simulation results

Fig. 4 (a) Images showing the impact dynamics of the droplets with five different impact velocities on smooth surfaces: (i) $V_0 = 0.1$ m/s, (ii) 0.2 m/s, (iii) 0.3 m/s, (iv) 0.4 m/s, and (v) 0.5 m/s. Red area indicates the distribution of liquid phase. The time evolution of the spreading factor of droplet collision: (b) the first oscillation cycle and (c) the oscillation within 100 ms

the normal momentum of droplet changes abruptly but not instantaneously due to the retardation of solid surface. With the decrease of droplet height, the lower part of the droplet forms a outward radial flow (see t = 2.0 ms). Subsequently, the wetting area increases gradually with the growth of the radial flow. Until t = 6.2 ms, this flow achieves the maximum wetting area in which the major driving forces for droplet movement become capillary forces. Accordingly, the spreading factor β increase to the maximum spreading factor of $\beta_{max} = 2.43$, as shown

in Fig. 4(b). After that, the droplet retracts inward, and the droplet height rises from the center. At this point, the cohesive force of droplet forces the reduction of the wetting area, and the value of β begins to reduce. Under the combined effects of the surface tension and the developed inertia force (during the recoiling stage), the droplet raises to a certain height without bouncing-off at t = 13.8 ms, and the β reduce to the minimum value of 0.74. In the subsequent movement, gravity produces a downward flow, which makes the water droplet fall down. At time t = 19.8 ms, the droplet gets to the current maximum extent again. This oscillation process of the droplet advancing/ receding on a smooth surface continues until the droplet is at equilibrium, with time even beyond 400.0 ms. Similar spreading and receding processes are observed in the cases of $V_0 = 0.2$ m/s, 0.3 m/s and 0.4 m/s (see Fig. 4(a)-ii, iii, iv), but the time nodes are different. As presented in Fig. 4(b), the values of β_{max} for the three cases mentioned above are approximately 2.58/6.4 ms, 2.77/6.6 ms and 3.14/7.6 ms, respectively. Moreover, the major difference is the presence of the bending interface at droplet centre compared with $V_0 = 0.1$ m/s. For $V_0 = 0.5$ m/s (see Fig. 4(a)-v), a hole appears on the droplet centre due to the pinch-off of the bending interface, and the corresponding β_{max} is equal to 3.48 at time t = 8.2 ms. For these varying impact velocities during our test cases, the value of β_{max} is larger for higher values of V_0, and the spreading time corresponding to the β_{max} becomes longer. The reason is, as the value of V_0 increases, the initial kinetic energy of the droplet is higher under other constant conditions.

In order to quantitatively describe the oscillation characteristics of droplet deformation, Fig. 4(c) shows the time evolution of the spreading factor within time 100.0 ms for the varying impingement velocities. We would like to stress here that the variation of the spreading factor β within 100 ms is enough for us to identify the key features of oscillation characteristics (i.e., average amplitude ratio χ and average oscillation period ratio τ). For all values of V_0, the droplets undergo several damped oscillations on a flat smooth surface. The main point to stress here is that the dissipation action of viscosity will continue to weaken the oscillation until the droplet reaches equilibrium state. It is clear that the vibration amplitude is stronger as the magnitude of V_0 increases. With the magnitude of V_0 varying from 0.1 m/s to 0.5 m/s, the value of χ achieved during our VOF simulations is successively 1.045, 1.052, 1.058, 1.064 and 1.076. Similarly, the corresponding value of τ is 13.32 ms, 13.62 ms, 14.64 ms, 15.66 ms and 17.12 m. Therefore, both average amplitude ratio χ and average oscillation period ratio τ increase as the value of impact velocity increases. This is obvious, the above results instruct us that the

increase of impact velocity is unfavorable to weaken the droplet oscillation.

Effects of Wall Wettability on the Droplet Oscillation

Apart from impact velocity, wall wettability also plays a significant role in the dynamic behaviors of droplet collisions. The contact angle at which a liquid/vapor interface meets the solid surface is commonly used to characterize the ability of a liquid droplet to wet a solid surface. For a droplet resting on an ideal flat surface, this contact angle is called the static contact angle θ_E. For lower values of θ_E (e.g. $\theta_E < 90°$), the droplet tends to stick on wall surfaces due to the stronger wall adhesion. If the value of θ_E is higher (e.g. $\theta_E > 150°$), the droplet easily breaks up, fractures or rebounds because of the less wall resistance. Hence, the surface with the contact angle less than 90° is called the hydrophilic surface, while greater than 90° for the hydrophobic surface. However, the interface kinetics reveal that the contact angle is time-varying around the static contact angle θ_E on the dynamic processes of a droplet advancing and receding on a surface. Such contact angle is known as the dynamic contact angle θ_D, which is closely related to the velocity of the contact line. But in this section, we assume that the contact angle of the droplet moving on a smooth surface is a constant value which is equal to the static contact angle θ_E. A series of impingement simulations are performed to investigate the effects of wall wetting features with the static contact angle ranging from $\theta_E = 70°$ to 110° (involving from partial wetting to non-wetting). Here, we mainly examine the oscillation features of the droplet with $D_0 = 1.6$ mm moving on different smooth surfaces at both the low impact velocity ($V_0 = 0.2$ m/s) and the relatively high velocity ($V_0 = 0.4$ m/s) conditions. The free-slip boundary is imposed on the bottom edge of computational domain.

Figure 5(a) shows the images at various times for impact dynamics of the droplet with $V_0 = 0.2$ m/s (weakened spreading) on the ideal smooth surfaces with different wetting features. In the process of droplet spreading, velocity vector fields colored by velocity magnitude are also shown. Observing all these images, a oscillation behavior of the droplet advancing and recoiling can be easily obtained. It is obvious that with the increase of the θ_E value, the maximum wetting length gets reduced. For the lower values of θ_E (see Fig. 5(a) i, ii, iii, i.e., $\theta_E = 70°, 80°, 90°$), the formation of the bending interface at the droplet center can also be observed. It shows that the bending interface gets weakened as the value of θ_E is higher (e.g. $\theta_E = 100°$). For $\theta_E = 110°$, the bending interface is not formed at the droplet center due to the weak interaction between the wall surface and the
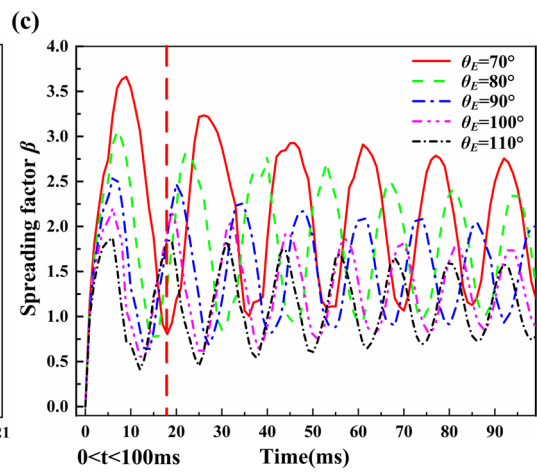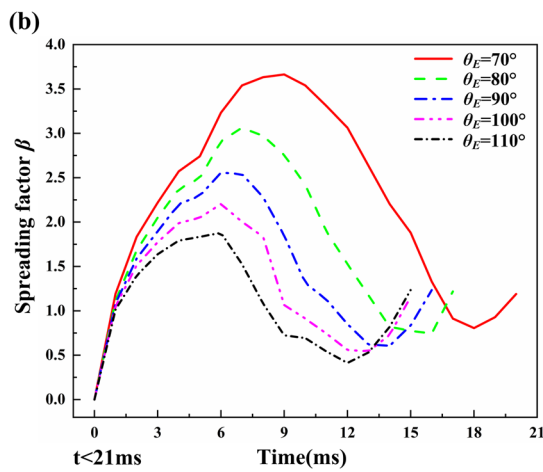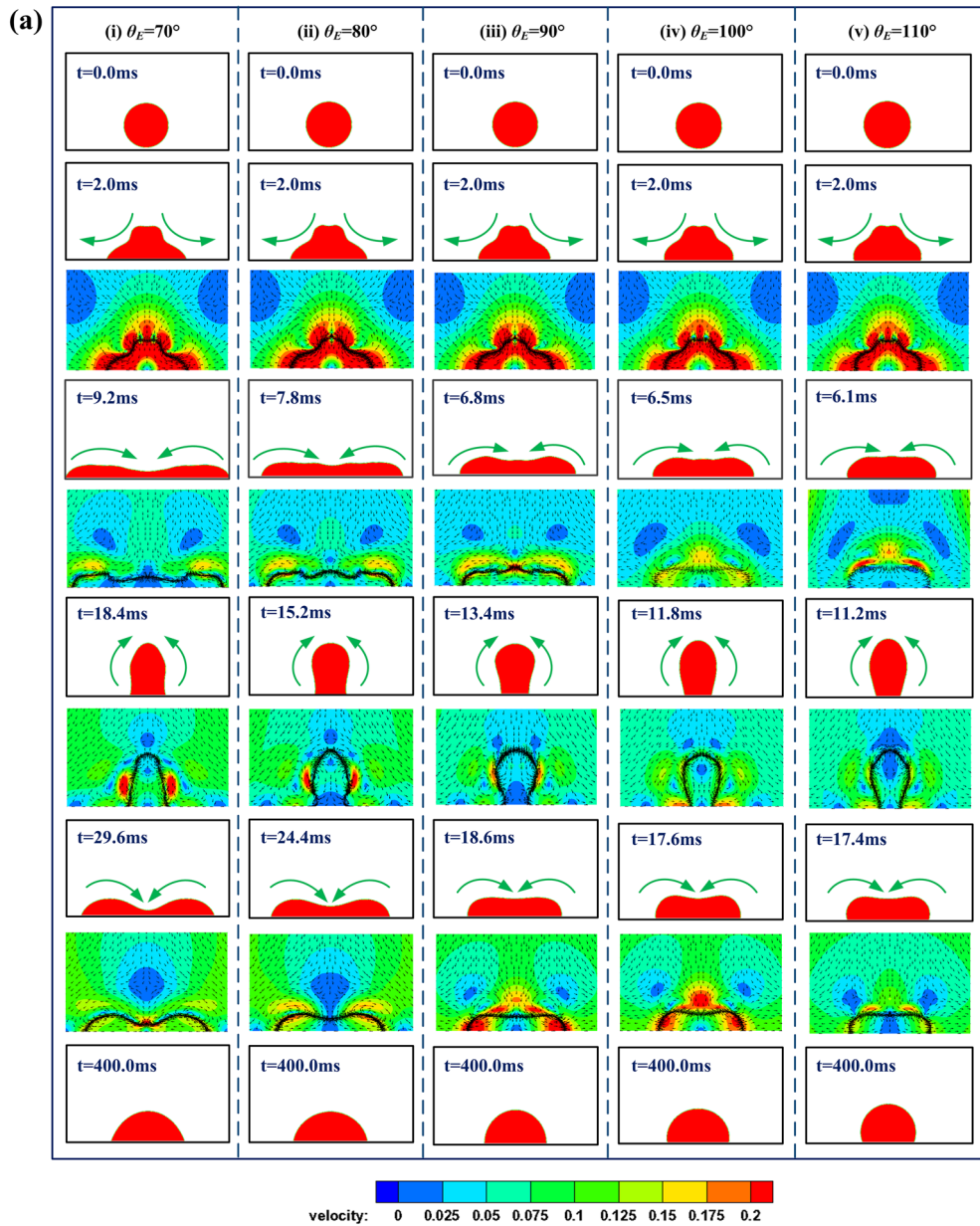
(a)

(i) $\theta_E = 70°$ (ii) $\theta_E = 80°$ (iii) $\theta_E = 90°$ (iv) $\theta_E = 100°$ (v) $\theta_E = 110°$

velocity: 0 0.025 0.05 0.075 0.1 0.125 0.15 0.175 0.2

(b)

Spreading factor β

Time(ms)

t<21ms

$\theta_E = 70°$
$\theta_E = 80°$
$\theta_E = 90°$
$\theta_E = 100°$
$\theta_E = 110°$

(c)

Spreading factor β

Time(ms)

0<t<100ms

$\theta_E = 70°$
$\theta_E = 80°$
$\theta_E = 90°$
$\theta_E = 100°$
$\theta_E = 110°$

◄**Fig. 5** (a) Images showing the impact dynamics of the droplet with $V_0 = 0.2$ m/s on the smooth surfaces with different wetting features: (i) $\theta_E = 70°$, (ii) 80°, (iii) 90°, (iv) 100°, and (v) 110°. Red area indicates the distribution of liquid phase. Velocity contour and velocity vectors colored by velocity magnitude are also plotted. The time evolution of the spreading factor of droplet collision: (b) the first oscillation cycle and (c) the oscillation within 100 ms

liquid droplet, as shown in Fig. 5(a)-iv, v. For the droplet shape at equilibrium state, the case with smaller θ_E value (e.g. $\theta_E = 70°$) has a larger static wetting area. Figure 5(b) presents the first oscillation cycle of the spreading factor β. For any droplet, the variation of β value increases firstly and then reduces with time. We can study the corresponding maximum value β_{max}. The value of β_{max} achieved during the first cycle for θ_E which ranges from 70° to 110° with the increment of 10 is found to be 3.66/9.2 ms, 3.06/7.8 ms, 2.55/6.8 ms, 2.21/6.5 ms and 1.87/6.1 ms, respectively. Hence, the β_{max} is larger for the smaller value of θ_E (e.g. $\theta_E = 70°$), and the spreading time corresponding to the β_{max} is longer. This is because the smaller value of θ_E corresponds to the stronger wall adhesion, which boosts the droplet wetting and causes β_{max} to become larger. Figure 5(c) shows the corresponding time evolution of the spreading factor β within time 100 ms for the varying contact angles at $V_0 = 0.2$ m/s. Several oscillation cycles of a droplet advancing and recoiling can be clearly observed. Overall parameters during the oscillation processes such as average amplitude ratio χ and average oscillation period ratio τ are approximately 1.051/17.1 ms, 1.050/15.2 ms, 1.049/13.7 ms, 1.041/12.7 and 1.028/12.6, respectively. It indicates that with the increase of θ_E value, both the values of χ and τ are reduced. We next study the oscillation features of droplet impact at $V_0 = 0.4$ m/s (forced spreading).

Figure 6(a) shows the images at various times for impact dynamics of the droplet with $V_0 = 0.4$ m/s on the ideal smooth surfaces with different wetting features. The calculated velocity fields regarding the droplet deformation behavior are also presented for the interpretation of spreading-receding phenomena that are observed in the VOF simulations. Overall deformation behaviors at $V_0 = 0.4$ m/s are similar to the corresponding cases of the previously obtained droplet impacts at $V_0 = 0.2$ m/s on the ideal smooth surfaces with different contact angles. Compared Fig. 6(a) with Fig. 5(a), the main differences are the pinch-off of bending interface and the presence of a nearly bouncing-off in the group of forced spreading. As indicated in Fig. 6(b), the value of β_{max} obtained during the first cycle for θ_E value varying from 70° to 110° is found to be 4.57/10.6 ms, 3.71/8.8 ms, 3.14/7.4 ms, 2.69/6.6 ms and 3.32/6.2 ms, respectively. Figure 6(c) also shows oscillation processes of the spreading factor β within time 100 ms for the varying contact angles. It can be seen that the oscillations at

$V_0 = 0.4$ m/s show the stronger vibration amplitude and the smaller oscillation frequency than at $V_0 = 0.2$ m/s. The values of χ and τ are 1.102/19.2 ms, 1.074/16.7 ms, 1.073/15.7 ms, 1.069/14.2 ms and 1.067/14.1 ms, respectively. Here, we summarize that the droplet impacting on a hydrophobic surface may show a oscillation with the short oscillation cycle and the slow attenuation compared the collision on a hydrophilic surface.

Combined Fig. 5 with Fig. 6, both groups (i.e. $V_0 = 0.2$ m/s and 0.4 m/s) show that the reduction of θ_E can contribute to damping the oscillation amplitude of the droplet, and delaying the average oscillation period. An important point to remember is that for the case of the droplet with relatively small velocity (e.g. $V_0 = 0.05$ m/s) impacting onto a relatively hydrophilic surface (e.g. $\theta_E = 10°$), the oscillation process may be quite weak. The above results instruct us that the decrease of contact angle is prone to weaken the droplet oscillation, but with a larger wetting area.

Effects of Slip Length λ on the Droplet Oscillation

The slip boundary condition states a velocity discontinuity at the solid–fluid interface. Hence there is a slip movement between the fluid and the boundary. Hydrodynamics indicates that the slip boundary condition is able to prevent the stress singularity problems of a moving three-phase contact line. The slip length λ is a hypothetical distance inside of the boundary at which the fluid velocity at the solid–fluid interface effectively come to the velocity of the boundary. The related research shows that a smaller value of slip length λ may correspond to higher interface energy dissipation. In order to make our conclusion more general, two groups, $V_0 = 0.2$ m/s/$\theta_E = 70°$ and $V_0 = 0.4$ m/s/$\theta_E = 110°$, are used to fully explain the effects of the slip length λ on the droplet oscillation features. More specifically, we use five different boundary conditions: $\lambda = 0.005$ mm, 0.2 mm, 0.4 mm, 0.8 mm and free-slip in the VOF calculations. Here, a water droplet with diameter $D_0 = 1.6$ mm is selected as the experimental fluid.

Figure 7 shows the time evolution of droplet impact diffusion factor on smooth surface under different boundary conditions when $V_0 = 0.2$ m/s/$\theta_E = 70°$ and $V_0 = 0.4$ m/s/$\theta_E = 110°$, respectively. The purpose of our arrangement is to verify the result consistency of two groups: the near capillary spreading ($V_0 = 0.2$ m/s/$\theta_E = 70°$) and the near bouncing-off ($V_0 = 0.4$ m/s/$\theta_E = 110°$). In this figure, the time evolution (i), as shown in the schematic on the left hand side of Fig. 7, is used to present the first oscillation cycle, which is in favor of describing the droplet deformation. A similar curve with the oscillation variation of droplet spreading is observed for either the near capillary spreading or the near bouncing-off in Fig. 7. It can be seen that the oscillation amplitude of β is higher
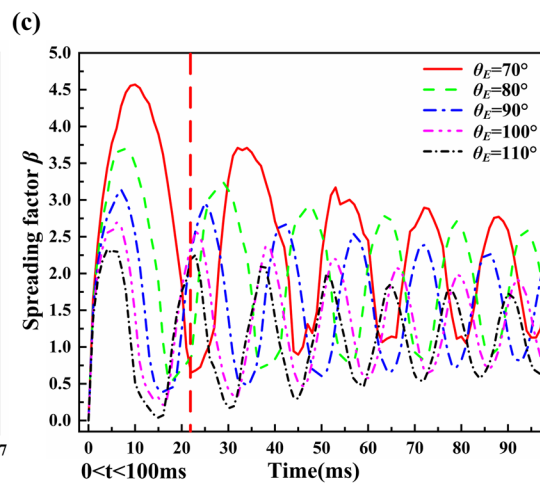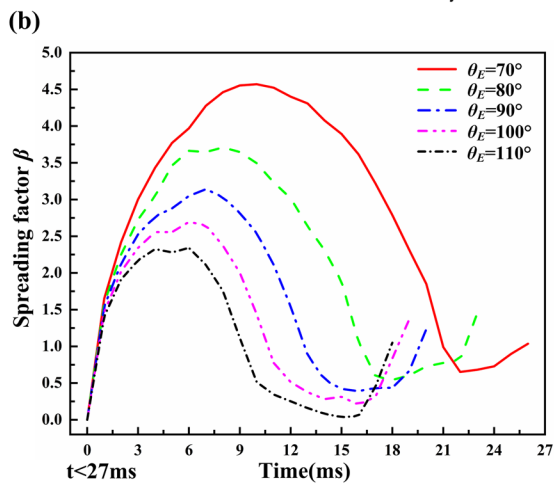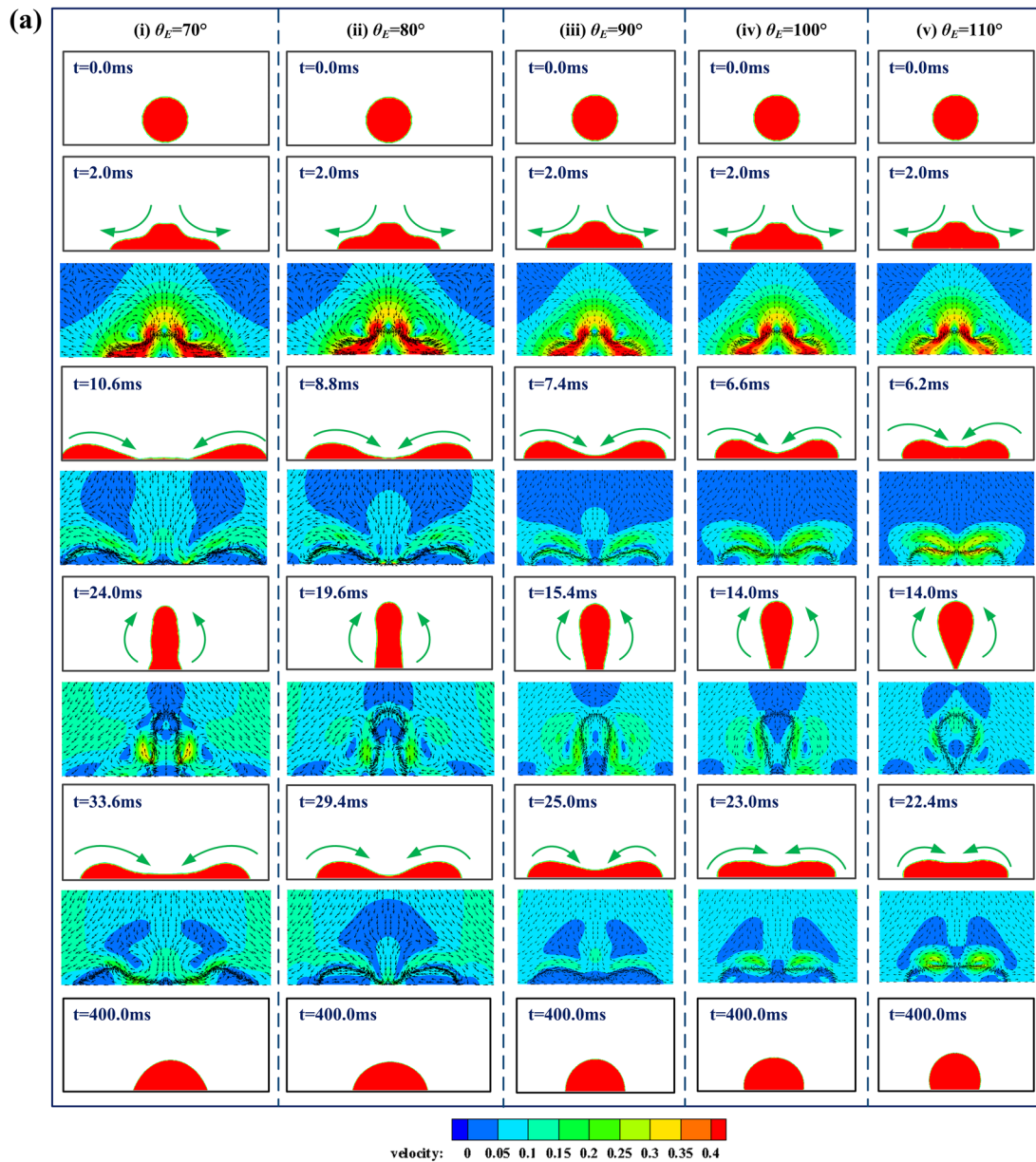
◄**Fig. 6** (a) Images showing the impact dynamics of the droplet with $V_0 = 0.4$ m/s on the smooth surfaces with different wetting features: (i) $\theta_E = 70°$, (ii) 80°, (iii) 90°, (iv) 100°, and (v) 110°. Red area indicates the distribution of liquid phase. Velocity contour and velocity vectors colored by velocity magnitude are also plotted. The time evolution of the spreading factor of droplet collision: (b) the first oscillation cycle and (c) the oscillation within 100 ms

for the near capillary spreading than that for the near bouncing-off. Both Fig. 7(a)-i and Fig. 7(b)-i exhibit that the evolution value of β varies slightly for these different boundary conditions considered here under the first oscillation cycle. After the first oscillation cycle, the boundary slip markedly changes the average period and average amplitude of the droplet oscillation, especially in the group $V_0 = 0.2$ m/s/$\theta_E = 70°$ (see Fig. 7(a)-ii). The reason is that the smaller slip length causes more energy loss at the

larger spreading area. Within time 100 ms of excluding the first oscillation cycle in Fig. 7(a)-ii, the oscillations indicate that average amplitude ratio χ and average oscillation period ratio τ are 1.073/14.7 ms, 1.066/15.7 ms, 1.064/16.1 ms, 1.056/16.7 ms and 1.054/17.3 ms for boundary conditions varying from λ = 0.05 mm to freeslip. The value of χ for λ = 0.05 mm is 2% less than that for free-slip condition, and the value of τ is reduced by 15%. This implies that with the reduction of λ value, the oscillation stage vanishes more rapidly. For Fig. 7(b)-ii, the values of χ and τ are 1.074/13.7 ms, 1.073/13.7, 1.066/14.1 ms, 1.064/14.2 ms, and 1.063/14.2 ms, respectively. Both Fig. 7(a) and Fig. 7(b) show that the value of boundary slip λ gets smaller, the liquid shear rate at the solid–fluid interface is more prominent, which will be more effective for the suppression of the droplet oscillation.
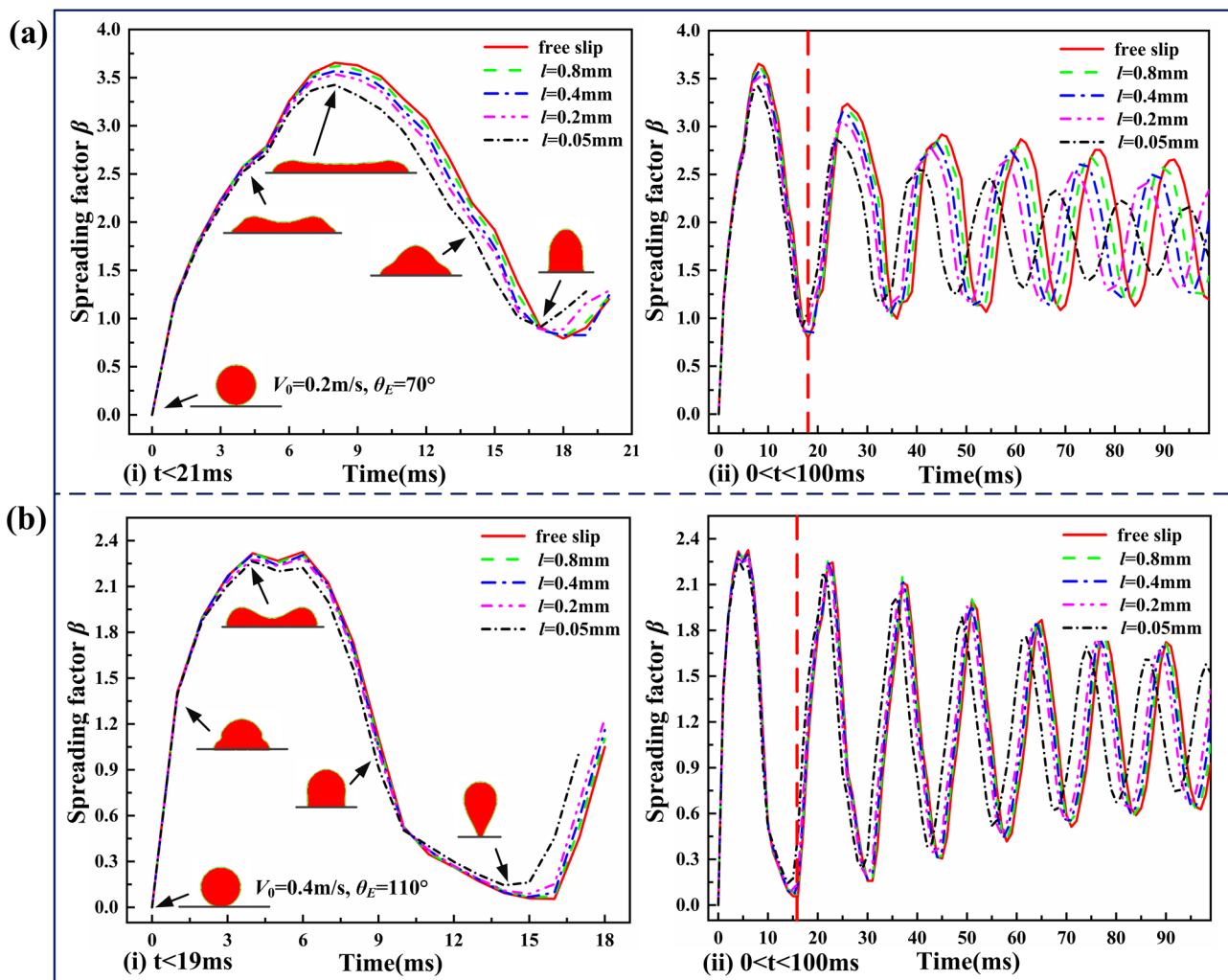

Fig. 7 Time evolution of the spreading factor of a droplet impacting on the smooth surfaces with different boundary conditions (i.e., λ = 0.05 mm, 0.2 mm, 0.4 mm, 0.8 mm, and free-slip) for (a) $V_0 = 0.2$ m/s and $\theta_E = 70°$, and (b) $V_0 = 0.4$ m/s and $\theta_E = 110°$. As shown in the schematic, the left hand (i) indicate the first oscillation cycle and the right hand (ii) is the oscillation within 100 ms

Effects of Surface Tension on the Droplet Oscillation

Surface tension results from the enhancement of the inward attractive forces between like molecules residing at or close to the interface. When a droplet starts spreading on a smooth surface with the creation of new surfaces, the initial kinetic energy of drop impact is partly dissipated by the viscous forces, and partly converts into the surface energy (free-surface area) and adhesion energy (liquid–solid contact area). It is clear that the subsequent behavior of the droplet is largely related to the competition between the surface energy and the adhesion energy. If the droplet with sufficient surface energy overcomes the less adhesion energy while the droplet recoiling, droplet bouncing-off may

occur instead of droplet depositing. Therefore, the surface tension also plays a vital role in sculpting the outcomes of drop impact. In this study, we also separate the deformation degree of a water droplet impacting on the smooth surface into two groups: the near capillary spreading ($V_0 = 0.2$ m/s$/\theta_E = 70°$) and the near bouncing-off ($V_0 = 0.4$ m/s$/\theta_E = 110°$). In order to study the effect of surface tension, the density and viscosity of water ($D_0 = 1.6$ mm) are kept constant, while surface tension is varied for simulation requirements. Five different surface tensions are studied for $\gamma_{LV} = 0.095$ N·m^{-1}, 0.085 N·m^{-1}, 0.075 N·m^{-1}, 0.065 N·m^{-1}, and 0.055 N·m^{-1} in each group. In addition, the free-slip boundary is select as the boundary condition.

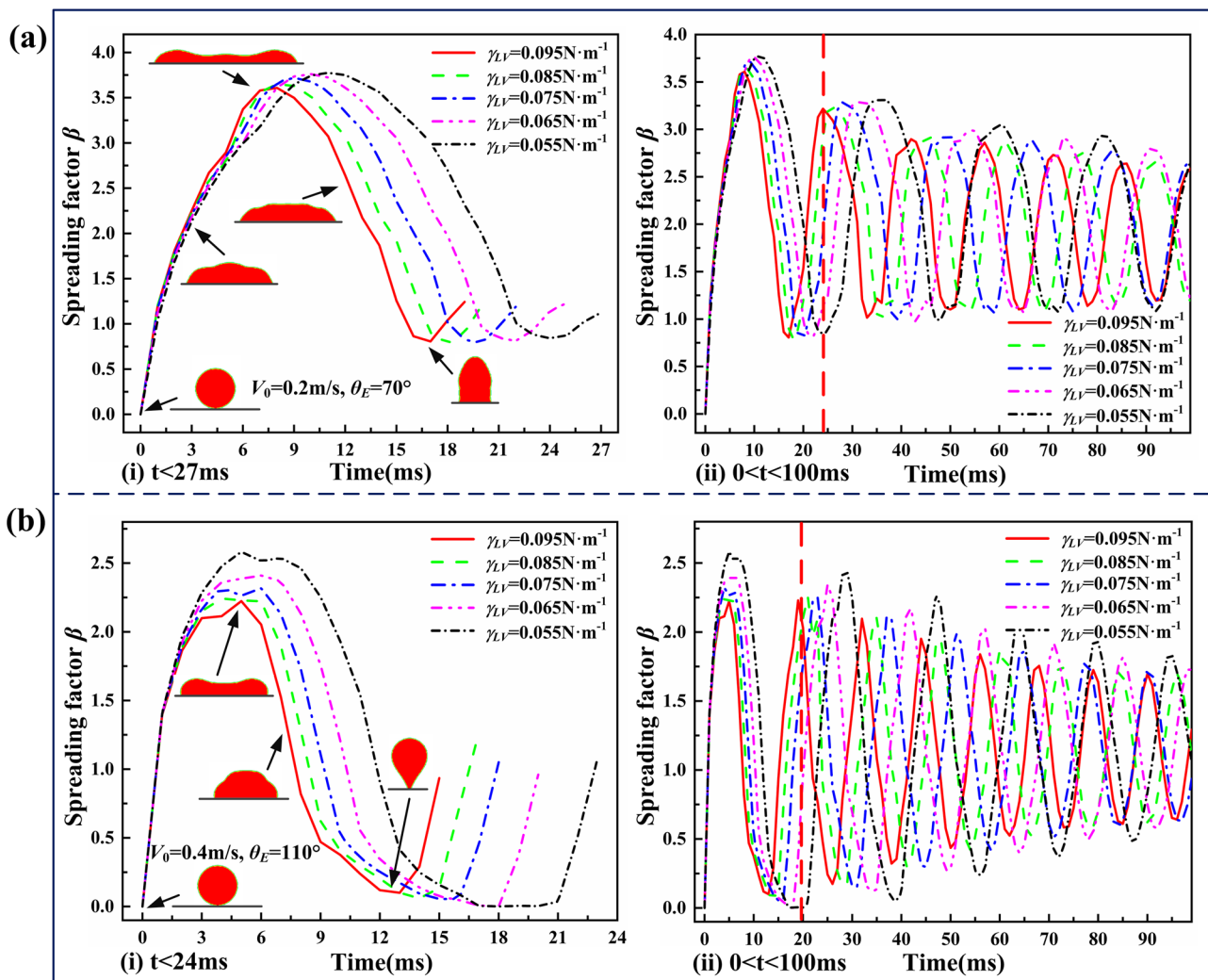**Fig. 8** Time evolution of the spreading factor of droplets with different surface tensions (i.e., $\gamma_{LV} = 0.095$ N·m^{-1}, 0.085 N·m^{-1}, 0.075 N·m^{-1}, 0.065 N·m^{-1}, and 0.055 N·m^{-1}) impacting on smooth surfaces for (a) $V_0 = 0.2$ m/s and $\theta_E = 70°$, and (b) $V_0 = 0.4$ m/s and $\theta_E = 110°$. As shown in the schematic, the left hand (i) indicate the first oscillation cycle and the right hand (ii) is the oscillation within 100 ms

Figure 8(a) shows the time evolution of the spreading factor β of droplet impacting on the smooth surface for varying surface tensions in the group of $V_0 = 0.2$ m/s/$\theta_E = 70°$. It is found that surface tension has a significant effect on the droplet oscillation. As shown in Fig. 8(a)-i, the spreading feature is almost the same for all cases, but the maximum spreading factor β_{max} is smaller for larger surface tension (e.g. $\gamma_{LV} = 0.085$ N·m^{-1}). Figure 8(a)-ii shows that the curves of different surface tensions depart each other after the first spreading/recoiling cycle. The average amplitude ratio χ and the average oscillation period ratio τ are 1.055/15.7 ms, 1.056/16.7 ms, 1.058/18.3 ms, 1.058/20.1 ms, and 1.063/22.5 ms for surface tension varying from 0.095 N·m^{-1} to 0.055 N·m^{-1}. These data indicate that both the average amplitude ratio χ and the average oscillation period ratio τ decrease with the increase of surface tension. This may be explained as due to the droplet with relatively higher surface tension (e.g. $_{LV} = 0.095$ N·m^{-1}) prevents droplet expanding, which leads to a relatively more rapid retraction with lower viscous dissipation.

On the other hand, for $V_0 = 0.4$ m/s/$\theta_E = 110°$ (see Fig. 8(b)), the average oscillation period and the average amplitude radio are further reduced due to the hydrophobic surface regardless of the increase in impact velocity, respectively. As shown in Fig. 8(b)-i, the droplet impacting on the hydrophobic surface nearly detaches from the smooth surface and makes the effect of surface tension more clear. Figure 8(b)-ii illustrates that for surface tension varying from 0.095 N·m^{-1} to 0.055 N·m^{-1}, the values of χ and τ are 1.064/12.7 ms, 1.065/13.1 ms, 1.066/14.1 ms, 1.068/15.3, and 1.071/16.7 ms, respectively. It can be found that surface tension can affect the oscillation features of the droplet impacting on the hydrophobic surface. Reduction of the average oscillation period is also associated with the increase of surface tension. On the hydrophobic surface, the reason of the relatively rapid retraction of the droplet with larger surface tension can be described by the increasing surface energy.

The above results instruct us that for impact on a hydrophilic surface, increasing the surface tension of droplet is beneficial to quicken the oscillation frequency, and decrease the oscillation magnitude. For impact on a hydrophobic surface, the droplet with smaller surface tension (e.g. $\gamma_{LV} = 0.065$ N·m^{-1}) can reduce the oscillation frequency and increase the wetting area.

Effects of Liquid Density ρ_L on the Droplet Oscillation

We now discuss the effects of liquid density ρ_L on the droplet oscillation. It is obvious that the density of the droplet is closely related to the inertial force of droplet spreading /recoiling. For VOF numerical simulations, the free-slip boundary is select as the boundary condition. A diameter $D_0 = 1.6$ mm of a water-like droplet impacting on a smooth surface is selected. We only vary the liquid density of the water-like form $\rho_L = 700$ kg·m^{-3} to 1100 kg·m^{-3}, with intermediate values 800 kg·m^{-3}, 900 kg·m^{-3}, 998 kg·m^{-3}. The choice of these values of liquid density refers to the density values of petrol, kerosene, mineral oil, water and ethylene glycol, respectively. Two different groups, $V_0 = 0.3$ m/s/$\theta_E = 70°$ and $V_0 = 0.2$ m/s/$\theta_E = 110°$, are used to get a better insight into the effects of liquid density ρ_L on the droplet oscillation.

Figure 9(a) exhibits the time evolution of the spreading factor β of water-liquid droplets with varying liquid density values impacting on smooth surfaces at the group of $V_0 = 0.2$ m/s/$\theta_E = 70°$. As plotted in Fig. 9(a)-i, the general variation of the spreading factor β is similar for all the considered liquid density values under the first oscillation cycle, but their peaks are different. The maximum spreading factor β_{max} appears to be significantly higher for larger liquid density (e.g. $\rho_L = 1100$ kg·m^{-3}). In Fig. 9(a)-ii, which depicts the corresponding droplet oscillations within 100 ms, the liquid density evidently changes the frequency and amplitude of the droplet oscillation. The oscillation parameters such as the average amplitude ratio χ and the average oscillation period ratio τ are 1.052/14.1 ms, 1.053/15.3 ms, 1.055/16.3 ms, 1.055/17.3 ms, and 1.061/18.3 ms for liquid density value ranging from 700 kg·m^{-3} to 1100 kg·m^{-3}. It can be found that the average oscillation period increases with the increase of liquid density. This is because the higher liquid density (e.g. $\rho_L = 1100$ kg·m^{-3}) corresponds to higher initial kinetic energy of the droplet, which boosts the droplet spreading due to larger inertial force and leads to the longer time of advancing stage. Additionally, the average amplitude ratio also raises. For another group of $V_0 = 0.2$ m/s/$\theta_E = 110°$ (see Fig. 9(b)), the values of χ and τ are 1.039/10.3 ms, 1.039/11.1 ms, 1.039/11.7 ms, 1.042/12.3 ms, and 1.043/13.3 ms, respectively. As expected, the average amplitude ratio and average oscillation period also increase with the increase of liquid density.

In this section, both of groups have similar oscillation features for different liquid density values. The only difference is that oscillations resulting from the group of $V_0 = 0.3$ m/s/$\theta_E = 70°$ are likely to have a lower oscillation frequency than those resulting from $V_0 = 0.2$ m/s/$\theta_E = 110°$ due to the strong interaction between the droplet and the wall surface. The main viewpoint is that a smaller liquid density might aid in faster convergence at the early stage of impact under other conditions being equal. But in turn, the increase of droplet density results in additional damping of the droplet movement, which may accelerate the oscillation attenuation at the end of the oscillation.
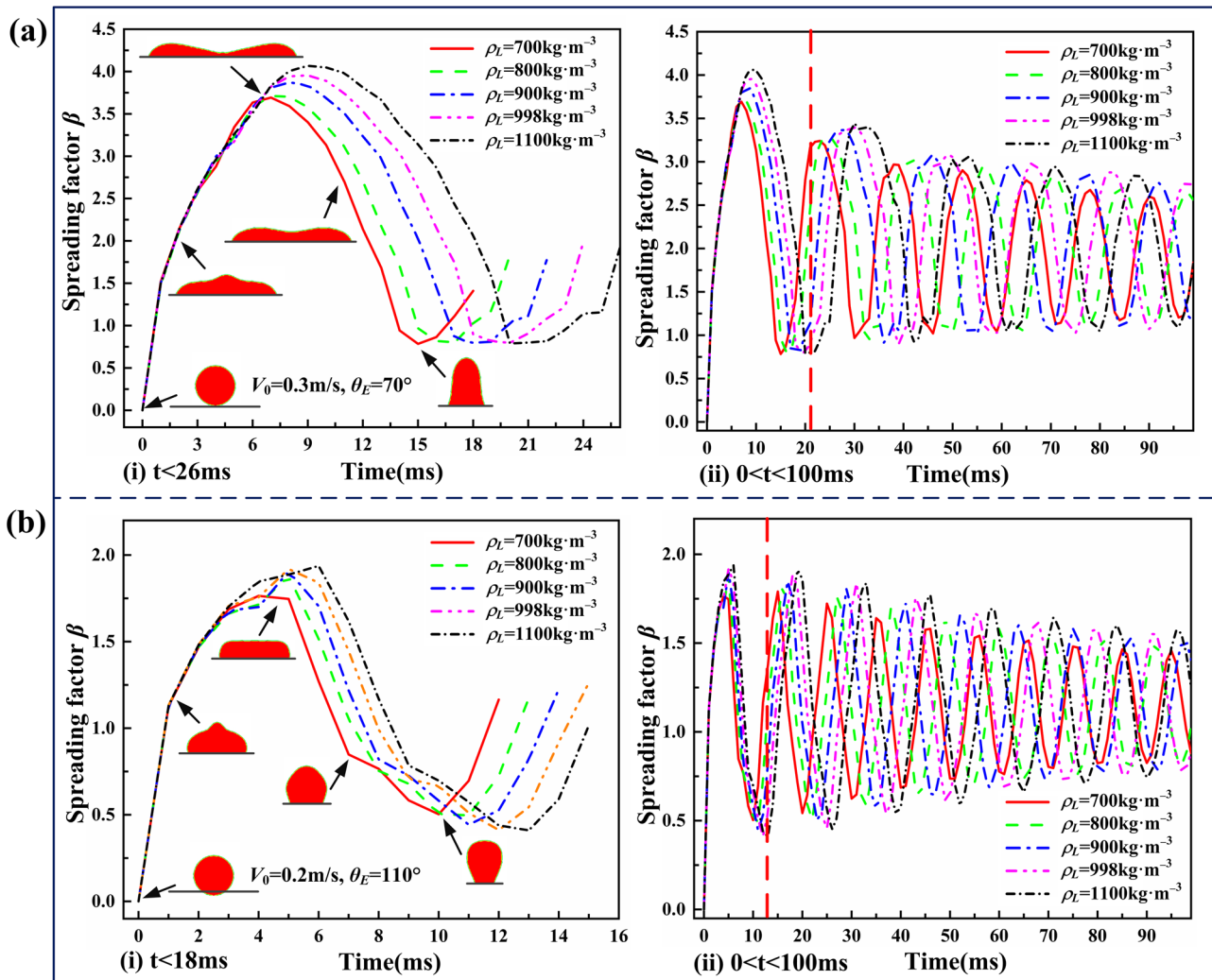
Fig. 9 Time evolution of the spreading factor of droplets with different liquid density values (i.e., $\rho_L = 700$ kg·m^{-3}, 800 kg·m^{-3}, 900 kg·m^{-3}, 998 kg·m^{-3}, and 1100 kg·m^{-3}) impacting on smooth surfaces for (a) $V_0 = 0.3$ m/s/$\theta_E = 70°$, and (b) $V_0 = 0.2$ m/s/$\theta_E = 110°$. As shown in the schematic, the left hand (i) indicate the first oscillation cycle and the right hand (ii) is the oscillation within 100 ms

Effects of Liquid Viscosity μ_L on the Droplet Oscillation

By following a similar procedure to that used in the previous investigation of liquid viscosity, influences of liquid viscosity on oscillation features of a water-like droplet advancing/recoiling onto both hydrophilic and hydrophobic surfaces also are examined separately. Also, we only vary the viscosity value of the water-like liquid form $\mu_L = 0.6$ N·s·m^{-3} to 4.0 N·s·m^{-3}, with intermediate values 0.8 N·s·m^{-3}, 1.003 N·s·m^{-3}, 2.5 N·s·m^{-3}. In the simulation, the effects of liquid viscosity on the oscillation behaviors of a droplet are inspected through the comparison and combination of two impact groups: (i) $V_0 = 0.3$ m/s/$\theta_E = 70°$ and (ii) $V_0 = 0.2$ m/s/$\theta_E = 110°$.

Droplet motion for each group is shown in Fig. 10. It can be seen that the oscillation arising from droplet spreading and

recoiling is similar for each impact group. For the first group, Fig. 10(a)-i shows that the maximum spreading factor β_{max} increases with the reduction of liquid viscosity. This is due to the fact that the higher value of viscosity (e.g. $\mu_L = 4.0$ N·s·m^{-3}) hinders the deformation rate, and is inclined to prevent the droplet movement. Figure 10(a)-ii indicates that the viscosity velocity has a significant influence on the droplet oscillation. The average amplitude ratio χ and the average oscillation period ratio τ are 1.066/18.1 ms, 1.060/18.0 ms, 1.057/17.3 ms, 1.090/15.3 ms, and 1.094/15.1 ms for liquid viscosity value ranging from 0.6 N·s·m^{-3} to 4.0 N·s·m^{-3}. It can be observed that a smaller liquid viscosity (e.g. $\mu_L = 0.6$ N·s·m^{-3}) yields a larger vibration amplitude, and correspondingly a longer average oscillation period. In case of viscosity value of 4.0 N·s·m^{-3}, the oscillation appears to be significantly faster than in the other cases. For the second group, the maximum
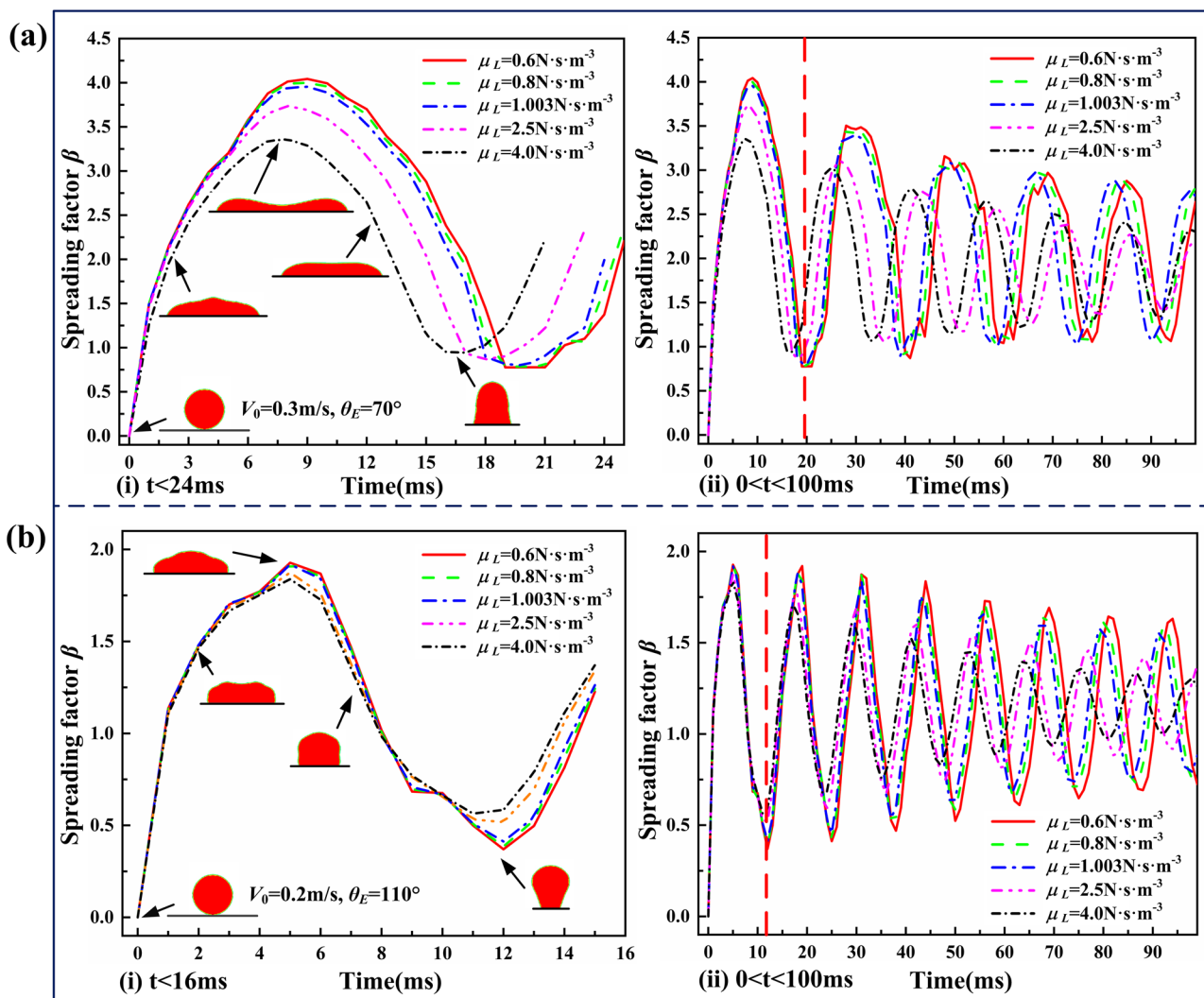
Fig. 10 Time evolution of the spreading factor of droplet with different liquid viscosity values (i.e., μ_L=0.6 N·s·m^{-3}, 0.8 N·s·m^{-3}, 1.003 N·s·m^{-3}, 2.5 N·s·m^{-3}, and 4.0 N·s·m^{-3}) impacting on smooth surfaces for (a) V_0=0.3 m/sθ_E=70°, and (b) V_0=0.2 m/sθ_E=110°. As shown in the schematic, the left hand (i) indicate the first oscillation cycle and the right hand (ii) is the oscillation within 100 ms

spreading factor β_{max} varies only slightly for all values of liquid viscosity, as shown in Fig. 10(b)-i. This phenomenon originates from the fact that surface tension plays a leading role at the first droplet spreading/recoiling cycle on hydrophobic surface. However, as time goes on, viscous dissipation becomes progressively more important, especially for a higher viscosity. Figure 10(b)-ii plots the time evolution of the spreading factor β within 100 ms at V_0=0.2 m/sθ_E=110° for varying values of liquid viscosity. Within time 100 ms of excluding the first oscillation cycle, the average amplitude ratio χ and the average oscillation period ratio τ are 1.035/12.7 ms, 1.042/12.3 ms, 1.044/12.3 ms, 1.044/11.7 ms, and 1.046/11.6 ms, respectively. This result again demonstrates that the droplet oscillation can be effectively suppressed by raising liquid viscosity. Hence, in summary, Fig. 10 suggests the droplet with relatively high viscosity (e.g. μ_L=4.0 N·s·m^{-3}) tends to dampen the droplet

oscillation on both hydrophilic and hydrophobic surfaces, especially in amplitude attenuation. However, for impact on hydrophobic surface, the droplet motion dominated by surface tension may greatly hinder the effect of viscosity within the first oscillation cycle (see Fig. 10(b)-i).

Effects of Droplet Diameter D_0 on the Droplet Oscillation

Considering that with the droplet size decreasing, surface tension gradually plays a more important role in droplet impact dynamics and may lead to different mechanisms of mass and energy transfer because of the scale effect. For this purpose, a water droplet colliding with a smooth surface is performed to study the effects of droplet diameter D_0 on the droplet oscillation features. In the VOF calculations,

we employ five different droplet diameters: $D_0 = 2.4$ mm, 2.0 mm, 1.6 mm, 1.2 mm, and 0.8 mm under free-slip boundary condition. Following a similar procedure, the exploration of two independent impact groups (i.e., (i) $V_0 = 0.3$ m/s/$\theta_E = 70°$ and (ii) $V_0 = 0.2$ m/s/$\theta_E = 110°$) are used to eliminate the deviation of droplet movement, which contributes to raise the reliability of conclusions.

Viewed as a whole in Fig. 11, the deformation of the droplet upon collision with the surface at diameter $D_0 = 2.4$ mm is relatively larger than that at $D_0 = 0.8$ mm for each group. Result for the impact group of $V_0 = 0.3$ m/s/$\theta_E = 70°$ is exhibited in Fig. 11(a) in terms of the time evolution of the spreading factor β of droplets with different droplet diameters impacting on smooth surfaces. Figure 11(a)-i shows that the spreading factor β

appears different trends. It can be seen that the value of β_{max} obtained during the first cycle for diameter value varying from $D_0 = 2.4$ mm to 0.8 mm is found to be 5.39/24.1 ms, 4.73/14.3 ms, 3.95/9.4 ms, 3.88/6.2 ms and 3.62/3.2 ms, respectively. The value of β_{max} is higher at larger values of droplet diameter (e.g. $D_0 = 2.4$ mm) compared to smaller values of droplet diameter (e.g. $D_0 = 0.8$ mm). This can be attributed to the fact that the influence of surface tension on the droplet spreading significantly increase with the increase of droplet size, so the wetting length is reduced a lot. Observing the oscillation process for all values of droplet diameter in Fig. 11(a)-ii, we obtain that the average amplitude ratio χ and the average oscillation period ratio τ are 1.263/45.7 ms, 1.190/31.7 ms, 1.099/19.3 ms, 1.098/12.3 ms, and 1.098/6.3 ms. It can be seen that with
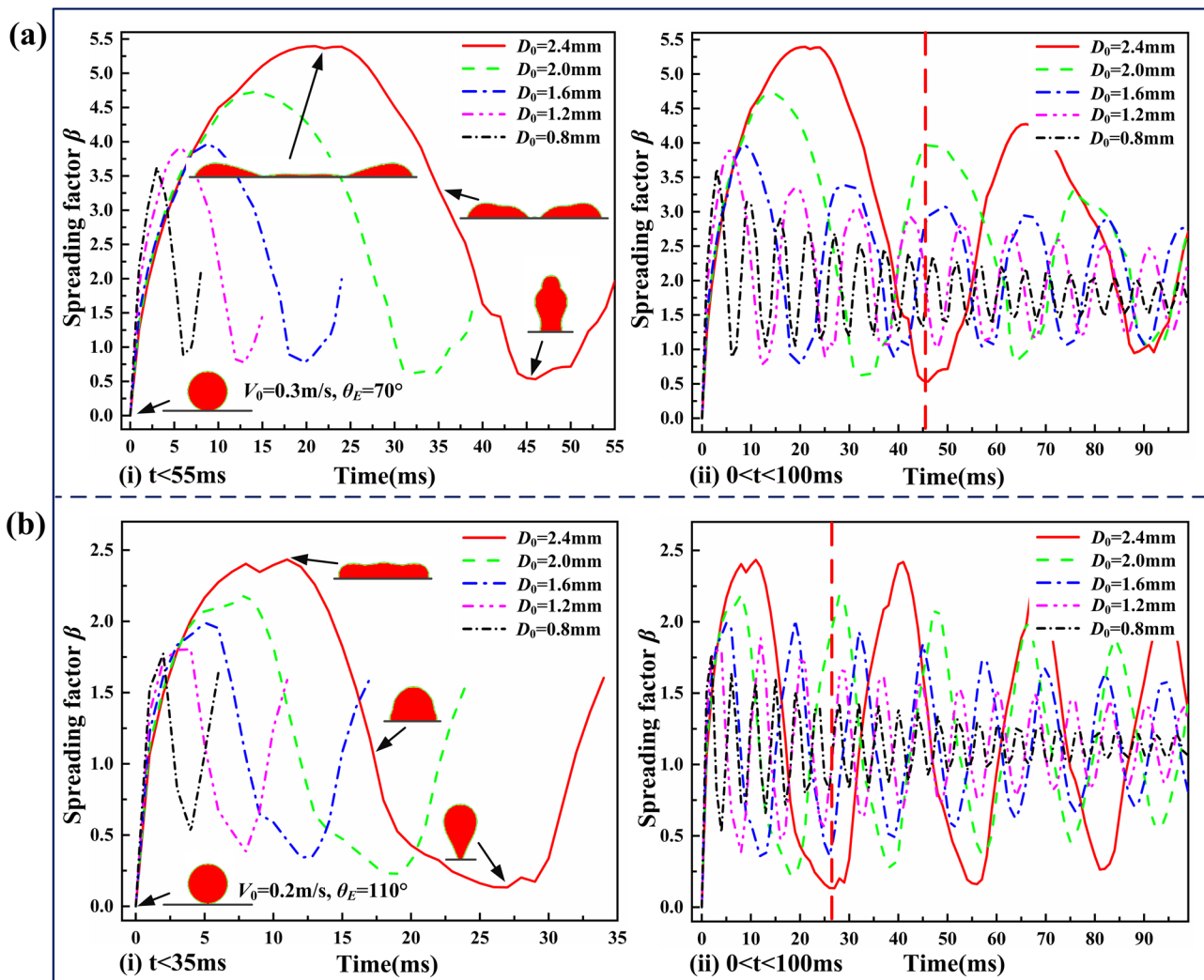

Fig. 11 Time evolution of the spreading factor of droplets with different droplet diameters (i.e., $D_0 = 2.4$ mm, 2.0 mm, 1.6 mm, 1.2 mm, and 0.8 mm) impacting on smooth surfaces for (a) $V_0 = 0.3$ m/s/$\theta_E = 70°$, and (b) $V_0 = 0.2$ m/s/$\theta_E = 110°$. As shown in the schematic, the left hand (i) indicate the first oscillation cycle and the right hand (ii) is the oscillation within 100 ms

the reduction of the droplet size, the initial kinetic energy decreases, and the effect of surface tension aggravates, the average oscillation period is greatly shortened.

On the other hand, for impact group of $V_0 = 0.2$ m/s/$\theta_E = 110°$, Fig. 11(b) illustrates the relation curves between the spreading factor β and the physical time at different droplet diameters. As shown in Fig. 11(b)-i, the deformations of droplets among these varying droplet diameters are markedly different. For instant, for the droplet with diameter $D_0 = 2.4$ mm, the maximum spreading factor β_{max} and its corresponding time are 2.43 and 11.2 ms, while 1.77 and 2.4 ms for the droplet diameter $D_0 = 0.8$ mm. As a whole, the maximum spreading factor β_{max} also increases with the increase of the droplet diameter. Figure 11(b)-ii describes that the spreading factor β within time 100 ms fluctuates periodically as the time increases. For diameter value varying from $D_0 = 2.4$ mm to 0.8 mm, the average amplitude ratio χ and the average oscillation period ratio τ are 1.051/26.5 ms, 1.052/18.7 ms, 1.053/12.7 ms, 1.064/11.1 ms, and 1.066/4.3 ms, respectively. Combined with Fig. 11(a) and Fig. 11(b), both of two groups narrate the same conclusion; that is, as the size of the falling droplet decreases, the spreading factor oscillates more rapidly, the peaks of the evolution curve of spreading factor with time become sharper, the average oscillation period gets smaller, making the change rate of droplet shape be more violent. Finally, we stress here that the size of droplet plays a very critical role in the droplet dynamics to control the droplet oscillation.

Conclusion

In this paper, VOF simulations have been performed to investigate the oscillation characteristics of the droplet advancing/receding on smooth surfaces. The dynamic adaptive mesh refinement is used to adaptively follow the small flow structures of the droplet spreading, which is conducive to increase calculation accuracy of the interaction among the gas, the falling liquid droplet, and the solid surface. The reliability of simulation results is validated by the previously reported experiments and then is applied to the implementation of the droplet oscillation rising from droplet advancing and receding on both hydrophilic and hydrophobic surfaces. Several key parameter ranges of the droplet impact dynamics are: impact velocity V_0: 0.1–0.5 m/s, contact angle θ_E: 70°-120°, slip length: 0.05–0.8 mm (and including free slip boundary condition), surface tension γ_{LV}: 0.055–0.095 N·m^{-1}, droplet density ρ_L: 700-1100 kg·m^{-3}, liquid viscosity μ_L: 0.6–4.0 N·s·m^{-3}, and droplet diameter D_0: 0.4–1.2 mm. We present a series of single-variant analysis for explaining the effect of these above-mention parameters on the droplet oscillation process. The detailed kinetic behaviors of droplet oscillating are analyzed quantitatively in terms of the variation of

spreading factor β with time (involving the average amplitude ratio χ and maximum spreading factor β_{max}) and the value of average oscillation period ratio τ. Some main conclusions of this study are obtained from VOF simulations below.

- VOF simulation results indicated that the impact velocity has a large influence on the variations of the spreading factor with time. With the impact velocity increasing from 0.1 m/s to 0.5 m/s, the average oscillation period increases, and the deformation degree of droplet also increases due to a more rapid change in the vertical velocity of fluid flow at the early stage of droplet impact.
- For wall adhesion, as the contact angle θ_E increases, the maximum spreading factor β_{max} gradually declines, and the average oscillation period decreases. In additional, the maximum spreading factor β_{max} tends to zero with θ_E rising up, which means that the droplet is subject to lift off the solid surface.
- For the cases of varying slip length, at lower values of slip length such as $\lambda < 0.05$ mm, the attenuation of the spreading factor β becomes more apparent as the droplet spreads on a hydrophilic surface. However, at higher values of slip length (involving free slip condition) such as $\lambda > 0.2$ mm, an increase in the slip length causes a slight variation of spreading factor β for both hydrophilic and hydrophobic surfaces.
- An increase in surface tension (keeping the contact angle constant) leads to a reduction of the average oscillation period because of the stronger cohesion of droplet. In addition, the maximum spreading factor β_{max} gradually decreases with the surface tension varying from 0.055 N·m^{-1} to 0.095 N·m^{-1}.
- The maximum spreading factor β_{max} shows an upward trend when the droplet density value goes from $\rho_L = 700$ kg·m^{-3} to 1100 kg·m^{-3}. Also, both the average amplitude ratio and the average oscillation period increase with the increase of liquid density. Because the higher liquid density corresponds to larger inertial energy and boosts the droplet spreading.
- As to the collisions at the value of liquid viscosity μ_L varying from $\mu_L = 0.6$ N·s·m^{-3} to 4.0 N·s·m^{-3}, for impact on hydrophobic surface, the droplet motion dominated by surface tension may greatly hinder the effect of viscosity at the early stage of impact. Generally, a higher fluid viscosity (e.g. $\mu_L = 4.0$ N·s·m^{-3}) hinders the droplet deformation, which leads to the lower average oscillation period and faster attenuation of amplitude compared a lower fluid viscosity (e.g. $\mu_L = 0.6$ N·s·m^{-3}) in terms of spreading factor β.
- The droplet diameter plays a significant role in droplet dynamics. Two significant differences are observed with respective to the influence of droplet size. First, the maximum spreading factor β_{max} varies significantly with

physical time as the droplet diameter rises up. Secondly, the average oscillation period reduces dramatically with the decrease of droplet diameter. This reduction may be explained as due to the scale effect with regard to surface tension.

Author Contribution Zongjun Yin: Data curation, Formal analysis, Writing—original draft. **Rong Su:** Validation, Software. **Wenfeng Zhang:** Conceptualization, Project administration, Writing—review & editing. **Zhenglong Ding:** Funding acquisition, Validation. **Qiannan Chen:** Validation, Software. **Futong Chai:** Investigation, Data curation. **Qingqing Wang:** Validation, Software. **Fengguang Liu:** Project administration.

Declarations

Declaration of Competing Interest The authors declare that they have no known competing financial interests or personal relationships that could have appeared to influence the work reported in this paper.

References

Antonini, C., Amirfazli, A., Marengo, M.: Drop impact and wettability: From hydrophilic to superhydrophobic surfaces. Phys. Fluids **24**(10), 102104 (2012). https://doi.org/10.1063/1.4757122

Alabuzhev, A.A.: Forced Axisymmetric Oscillations of a Drop, which is Clamped Between Different Surfaces. Microgravity Sci. Technol. **32**, 545–553 (2020). https://doi.org/10.1007/s12217-020-09783-2

Blake, T.D., De Coninck, C.: The influence of solid-liquid interactions on dynamic wetting. Adv. Colloid Interfac. **96**(1), 21–36 (2002). https://doi.org/10.1016/s0001-8686(01)00073-2

Bai, F., He, X., Yang, X., et al.: Three dimensional phase-field investigation of droplet formation in microfluidic flow focusing devices with experimental validation. Int. J. Multiphas. Flow **93**, 130–141 (2008). https://doi.org/10.1016/j.ijmultiphaseflow.2017.04.008

Bird, J.C., Dhiman, R., Kwon, H.M., et al.: Reducing the contact time of a bouncing drop. Nature **503**(7476), 385–388 (2013). https://doi.org/10.1038/nature12740

Blake, T.D.: The physics of moving wetting lines. J. Colloid Interf. Sci. **299**(1), 1–13 (2006). https://doi.org/10.1016/j.jcis.2006.03.051

Banitabaei, S.A., Amirfazli, A.: Droplet impact onto a solid particle: effect of wettability and impact velocity. Phys. Fluids **29**(6), 062111 (2017). https://doi.org/10.1063/1.4990088

Brandenbourger, M., Caps, H., Vitry, Y., et al.: Electrically Charged Droplets in Microgravity. Microgravity Sci. Technol. **29**, 229–239 (2017). https://doi.org/10.1007/s12217-017-9542-0

Cox, R.G.: The Dynamics of the Spreading of Liquids on a Solid Surface. Part 1. Viscous Flow, J. Fluid Mech. **168**(-1), 169–194 (1986). https://doi.org/10.1017/s0022112086000332

Chen, S., Phan-Thien, N., Fan, X.J., et al.: Dissipative particle dynamics simulation of polymer drops in a periodic shear flow. J. Non-Newtonian Fluid **118**(1), 65–81 (2004). https://doi.org/10.1016/j.jnnfm.2004.02.005

Dupont, J.B., Legendre, D.: Numerical simulation of static and sliding drop with contact angle hysteresis. J. Comput. Phys. **229**(7), 2453–2478 (2010). https://doi.org/10.1016/j.jcp.2009.07.034

Deepu, P., Chowdhuri, S., Basu, S.: Oscillation dynamics of sessile droplets subjected to substrate vibration. Chem. Eng. Sci. **118**, 9–19 (2014). https://doi.org/10.1016/j.ces.2014.07.028

Gilet, T., Bush, J.W.M.: Droplets bouncing on a wet, inclined surface. Phys. Fluids **24**(12), 122103 (2012). https://doi.org/10.1063/1.4771605

Guo, Y., Wei, L., Liang, G., et al.: Simulation of droplet impact on liquid film with CLSVOF. Int. J. Heat Mass Tran. **53**, 26–33 (2014). https://doi.org/10.1016/j.icheatmasstransfer.2014.02.00

Gong, S., Cheng, P.: Numerical simulation of pool boiling heat transfer on smooth surfaces with mixed wettability by lattice Boltzmann method. Int. J. Heat Mass Tran. **80**, 206–216 (2015). https://doi.org/10.1016/j.ijheatmasstransfer.2014.08.09

Gauthier, A., Symon, S., Clanet, C., et al.: Water impacting on super-rhydrophobic macrotextures. Nat. Commun. **6**(1), 8001 (2015). https://doi.org/10.1038/ncomms9001

Gunjal, P.R., Ranade, V.V., Chaudhari, R.V.: Dynamics of drop impact on solid surface: Experiments and VOF simulations. AIChE J. **51**(1), 59–78 (2005). https://doi.org/10.1002/aic.10300

Huh, C., Scriven, L.E.: Hydrodynamic model of steady movement of a solid/liquid/fluid contact line. J. Colloid Interf. Sci. **35**(1), 85–101 (1971). https://doi.org/10.1016/0021-9797(71)90188-3

Herbert, S., Fischer, S., Gambaryan-Roisman, T., et al.: Local heat transfer and phase change phenomena during single drop impingement on a hot surface. Int. J. Heat Mass Tran. **61**, 605–614 (2013). https://doi.org/10.1016/j.ijheatmasstransfer.2013.01.08

Hasan, M.N., Chandy, A., Choi, J.W.: Numerical analysis of post-impact droplet deformation for direct-print. Eng. Appl. Comp. Fluid **9**(1), 543–555 (2015). https://doi.org/10.1080/19942060.2015.1071526

Josserand, C., Thoroddsen, S.T.: Drop Impact on a Solid Surface. Annu. Rev. Fluid Mech. **48**, 365–391 (2016). https://doi.org/10.1146/annurev-fluid-122414-034401

Koplik, J., Zhang, R.: Nanodrop impact on solid surfaces. Phys. Fluids **25**(2), 022003 (2012). https://doi.org/10.1063/1.4790807

Kordilla, J., Tartakovsky, A.M., Geyer, T.: A smoothed particle hydrodynamics model for droplet and film flow on smooth and rough fracture surfaces. Adv. Water Resour. **59**, 1–14 (2013). https://doi.org/10.1016/j.advwatres.2013.04.009

Karimdoost-Yasuri, A., Passandideh-Fard, M.: On the microscopic parameters at a moving contact line during wetting process. Int. J. Surf. Sci. Eng. **7**(3), 197–216 (2013). https://doi.org/10.1504/ijsurfse.2013.056423

Lagrée, P.Y., Staron, L., Popinet, S.: The granular column collapse as a continuum: validity of a two-dimensional Navier-Stokes model with a μ(I)-rheology. J. Fluid Mech. **686**, 378–408 (2011). https://doi.org/10.1017/jfm.2011.335

Li, Z., Hu, G.H., Wang, Z.L., et al.: Three dimensional flow structures in a moving droplet on substrate: A dissipative particle dynamics study. Phys. Fluids **25**(7), 072103 (2013). https://doi.org/10.1063/1.4812366

Liu, Y., Andrew, M., Li, J., et al.: Symmetry-breaking in drop bouncing on curved surfaces. Nat. Commun. **6**(1), 10034 (2015). https://doi.org/10.1038/ncomms10034

Li, X.H., Zhang, X.X., Chen, M.: Estimation of viscous dissipation in nanodroplet impact and spreading. Phys. Fluids **27**(5), 052007 (2015). https://doi.org/10.1063/1.4921141

Liang, G., Mudawar, I.: Review of mass and momentum interactions during drop impact on a liquid film. Int. J. Heat Mass Tran. **101**, 577–599 (2016). https://doi.org/10.1016/j.ijheatmasstransfer.2016.05.062

Liang, G., Mudawar, I.: Review of drop impact on heated walls. Int. J. Heat Mass Tran. **106**, 103–126 (2017). https://doi.org/10.1016/j.ijheatmasstransfer.2016.10.03

Li, B.X., Li, X.H., Chen. M.: Spreading and breakup of nanodroplet impinging on surface. Phys. Fluids **29**(1), 012003 (2017). https://doi.org/10.1063/1.4974053

Li, D., Duan, X.: Numerical analysis of droplet impact and heat transfer on an inclined wet surface. Int. J. Heat Mass Tran. **128**, 459–468 (2019). https://doi.org/10.1016/j.ijheatmasstransfer.2018.09.02

Liang, G., Zhang, T., Chen, Y., et al.: Two-phase heat transfer of multi-droplet impact on liquid film. Int. J. Heat Mass Tran. **139**, 832–847 (2019a). https://doi.org/10.1016/j.ijheatmasstransfer.2019.05.055

Liang, G., Zhang, T., Chen, L., et al.: Single-phase heat transfer of multi-droplet impact on liquid film. Int. J. Heat Mass Tran. **132**, 288–292 (2019b). https://doi.org/10.1016/j.ijheatmasstransfer.2018.11.145

Li, H., Zhang, K.: Dynamic behavior of water droplets impacting on the superhydrophobic surface: Both experimental study and molecular dynamics simulation study. Appl. Surf. Sci. **498**, 143793 (2019). https://doi.org/10.1016/j.apsusc.2019.143793

Mukherjee, S., Abraham, J.: Crown behavior in drop impact on wet walls. Phys. Fluids **19**(5), 052103 (2007). https://doi.org/10.1063/1.2736085

Malgarinos, I., Nikolopoulos, N., Marengo, M., et al.: VOF simulations of the contact angle dynamics during the drop spreading: Standard models and a new wetting force model. Adv. Colloid Interfac. **212**(3), 1–20 (2014). https://doi.org/10.1016/j.cis.2014.07.004

Meng, S., Yang, R., Wu, J.S., et al.: Simulation of droplet spreading on porous substrates using smoothed particle hydrodynamics. Int. J. Heat Mass Tran. **77**, 828–833 (2014). https://doi.org/10.1016/j.ijheatmasstransfer.2014.05.056

Ma, T.Y., Zhang, F., Liu, H.F., et al.: Modeling of droplet/wall interaction based on SPH method. Int. J. Heat Mass Tran. **105**, 296–304 (2017). https://doi.org/10.1016/j.ijheatmasstransfer.2016.09.10

Pomeau, Y.: Recent progress in the moving contact line problem: a review. CR. Mecanique **330**(3), 207–222 (2002). https://doi.org/10.1016/s1631-0721(02)01445-6

Popinet, S.: Gerris: a tree-based adaptive solver for the incompressible Euler equations in complex geometries. J. Comput. Phys. **190**(2), 572–600 (2003). https://doi.org/10.1016/S0021-9991(03)00298-5

Popinet, S.: An accurate adaptive solver for surface-tension-driven interfacial flows. J. Comput. Phys. **228**(16), 5838–5866 (2009). https://doi.org/10.1016/j.jcp.2009.04.042

Rein, M.: Phenomena of liquid drop impact on solid and liquid surfaces. Fluid Dyn. Res. **12**(2), 61–93 (1993). https://doi.org/10.1016/0169-5983(93)90106-k

Rioboo, R., Marengo, M., Tropea, C.: Time evolution of liquid drop impact onto solid, dry surfaces. Exp. Fluids **33**(1), 112–124 (2002). https://doi.org/10.1007/s00348-002-0431-x

Ren, W., Weinan, E.: Boundary conditions for the moving contact line problem. Phys. Fluids **19**(2), 022101 (2007). https://doi.org/10.1063/1.2646754

Roisman, I.V., Opfer, L., Tropea, C., et al.: Drop impact onto a dry surface: Role of the dynamic contact angle. Colloids Surfaces A **322**(1–3), 183–191 (2008). https://doi.org/10.1016/j.colsurfa.2008.03.005

Šikalo, Š, Wilhelm, H.D., Roisman, I.V., et al.: Dynamic contact angle of spreading droplets: Experiments and simulations. Phys. Fluids **17**(6), 062103 (2005). https://doi.org/10.1063/1.1928828

Shen, S., Bi, F., Guo, Y.: Simulation of droplets impact on curved surfaces with lattice Boltzmann method. Int. J. Heat Mass Tran. **55**(23–24), 6938–6943 (2012). https://doi.org/10.1016/j.ijheatmasstransfer.2012.07.00

Sprittles, J.E., Shikhmurzaev, Y.D.: The dynamics of liquid drops and their interaction with solids of varying wettabilities. Phys. Fluids **24**(8), 082001 (2012). https://doi.org/10.1063/1.4739933

Sibley, D.N., Nold, A., Savva, N., et al.: A comparison of slip, disjoining pressure, and interface formation models for contact line motion through asymptotic analysis of thin two-dimensional droplet spreading. J. Eng. Math. **94**(1), 19–41 (2015). https://doi.org/10.1007/s10665-014-9702-9

Song, M., Liu, Z., Ma, Y., et al.: Reducing the contact time using macro anisotropic superhydrophobic surfaces: effect of parallel wire spacing on the drop impact. NPG Asia Mater. **9**(8), e415 (2017). https://doi.org/10.1038/am.2017.122

Worthington, A.M.: A Second Paper on the Forms Assumed by Drops of Liquids Falling Vertically on a Horizontal Plate. Proc. R. Soc. London **25**(171–178), 498–503 (1876). https://doi.org/10.1098/rspl.1876.0073

Wang, Y.B., Wang, X.D., Wang, T.H., et al.: Asymmetric heat transfer characteristics of a double droplet impact on a moving liquid film. Int. J. Heat Mass Tran. **126**, 649–659 (2018). https://doi.org/10.1016/j.ijheatmasstransfer.2018.05.161

Wang, X., Xu, B., Chen, Z., et al.: Effects of Gravitational Force and Surface Orientation on the Jumping Velocity and Energy Conversion Efficiency of Coalesced Droplets. Microgravity Sci. Technol. **32**, 1185–1197 (2020). https://doi.org/10.1007/s12217-020-09841-9

Xie, H., Zeng, Z., Zhang, L., et al.: Simulation on Thermocapillary-Driven Drop Coalescence by Hybrid Lattice Boltzmann Method. Microgravity Sci. Technol. **28**, 67–77 (2016). https://doi.org/10.1007/s12217-015-9483-4

Xu, B., Chen, Z.: Droplet Movement on a Composite Wedge-Shaped Surface with Multi-Gradients and Different Gravitational Field by Molecular Dynamics. Microgravity Sci. Technol. **30**, 571–579 (2018). https://doi.org/10.1007/s12217-018-9641-6

Xu, B., Chen, Z.: Condensation on Composite V-Shaped Surface with Different Gravity in Nanoscale. Microgravity Sci. Technol. **31**(5), 603–613 (2019). https://doi.org/10.1007/s12217-019-09731-9

Yarin, A.L.: DROP IMPACT DYNAMICS: Splashing, Spreading, Receding, Bouncing…. Annu. Rev. Fluid Mech. **38**(1), 159–192 (2006). https://doi.org/10.1146/annurev.fluid.38.050304.09214

Yuan, W., Zhang, L.: A Lattice Boltzmann Simulation of Droplet Impacting on Superhydrophobic Surfaces with Randomly Distributed Rough Structures. Langmuir **33**(3), 820–829 (2016). https://doi.org/10.1021/acs.langmuir.6b04041

Yin, C., Wang, T., Che, Z., et al.: Oblique impact of droplets on microstructured superhydrophobic surfaces. Int. J. Heat Mass Tran. **123**, 693–704 (2018). https://doi.org/10.1016/j.ijheatmasstransfer.2018.02.06

Yin, Z., Ding, Z., Ma, X., et al.: Molecular Dynamics Simulations of Single Water Nanodroplet Impinging Vertically on Curved Copper Substrate. Microgravity Sci. Technol. **31**(40), 749–757 (2019). https://doi.org/10.1007/s12217-019-9696-z

Yin, Z., Ding, Z., Zhang, W., et al.: Dynamic behaviors of nanoscale binary water droplets simultaneously impacting on flat surface. Comp. Mater. Sci. **183**, 109814 (2020). https://doi.org/10.1016/j.commatsci.2020.109814

Zhao, Y.: Moving contact line problem: Advances and perspectives. Theor. Appl. Mech. Lett. **4**(3), 034002 (2014). https://doi.org/10.1063/2.1403402

Zhu, L., Ge, J.R., Qi, Y.Y., et al.: Droplet impingement behavior analysis on the leaf surface of, shu-chazao, under different pesticide formulations. Comput. Electron. Agr. **144**, 16–25 (2018). https://doi.org/10.1016/j.compag.2017.11.030

Zhou, J., Wang, Y., Geng, J., et al.: Characteristic oscillation phenomenon after head-on collision of two nanofluid droplets. Phys. Fluids **30**, 072107 (2018). https://doi.org/10.1063/1.5040027